

# A unified framework for equation discovery and dynamic prediction of hysteretic systems

Siyuan Yang<sup>a</sup>, Wei Liu<sup>a,b</sup>, Zhilu Lai<sup>a,c,\*</sup>

<sup>a</sup>*Internet of Things Thrust, The Hong Kong University of Science and Technology (Guangzhou), China*

<sup>b</sup>*Department of Industrial Systems Engineering and Management, National University of Singapore, Singapore*

<sup>c</sup>*Department of Civil and Environmental Engineering, The Hong Kong University of Science and Technology, China*

---

## Abstract

Hysteresis is a nonlinear phenomenon with memory effects, where a system's output depends on both its current state and past states. It is prevalent in various physical and mechanical systems, such as yielding structures under seismic excitation, ferromagnetic materials, and piezoelectric actuators. Analytical models like the Bouc-Wen model are often employed but rely on idealized assumptions and careful parameter calibration, limiting their applicability to diverse or mechanism-unknown behaviors. Existing equation discovery approaches for hysteresis are often system-specific or rely on predefined model libraries, which limit their flexibility and ability to capture the hidden mechanisms. To address these challenges, this research classifies equation discovery problems for hysteretic systems and develops a unified framework in which the state-space form is reformulated, and hysteretic variables are treated as trainable parameters from data. The framework further employs symbolic regression (SR) to automatically recover explicit governing equations without relying on predefined libraries, unlike methods such as sparse identification of nonlinear dynamics (SINDy). Experimental results demonstrate that the proposed method is effective in recovering governing equations for hysteretic systems, even in a challenging *Full Equation Discovery* setting, where prior information is extremely limited, and solving the equations naturally enables the dynamic prediction of hysteretic systems.

---

\*Corresponding author.

*Email addresses:* syang724@connect.hkust-gz.edu.cn (Siyuan Yang), weiliu@u.nus.edu (Wei Liu), zhilulai@ust.hk (Zhilu Lai)

*Keywords:* Hysteretic dynamic systems; equation discovery; symbolic regression; hysteretic variable learning

---

## 1. Introduction

Hysteresis is a common nonlinear phenomenon observed in a broad spectrum of engineering and physical systems, including ferromagnetic materials [1], piezoelectric actuators [2], structural materials [3], damping devices [4, 5], and shape memory alloys [6]. Hysteresis, characterized by its path-dependent behavior, refers to systems in which the output depends not only on the current state but also its history, often appearing as input-output loops associated with energy dissipation and irreversible processes [7, 8]. In nonlinear dynamic systems, hysteresis presents significant challenges for modeling, control, and prediction, owing to its multivalued behavior, rate dependence, and sensitivity to input history. Accurately capturing hysteresis behavior is therefore crucial in applications such as structural health monitoring [9], smart material design [10], and precision actuation [11, 12].

In response to these needs, numerous mathematical models have been proposed over the past decades to characterize hysteretic behaviors. Among these, the Bouc-Wen model [7] has been widely used as a baseline in structural dynamics due to its compact differential representation and the ability of its parameter set to reproduce a range of smooth, rate-dependent hysteresis loops. Its parameters provide physical interpretability and offer flexibility in capturing both softening and hardening behaviors. Recent reviews and comparative works have emphasized that the classical Bouc-Wen formulation has well-known limitations when modeling more complex phenomena [13], including pronounced asymmetry, pinching, and strength/stiffness degradation. To address these, generalized Bouc-Wen models [14], and alternative phenomenological frameworks [15] have been developed and systematically compared in the recent literature [16]. In this research, the Bouc-Wen model is used primarily as a representative benchmark to motivate the subsequent equation discovery setting. These limitations motivate the need for more flexible, data-driven approaches that can infer governing equations directly from observed hysteretic responses.

In recent years, data-driven modeling has opened new venues for discovering governing laws directly from measured data [17–23], especially when governing mechanism of the system is unknown. The sparse identification of

nonlinear dynamics (SINDy) [24] has shown strong potential in extracting compact and interpretable dynamic equations, by applying sparse regression with a predefined library of candidate functions. Extensions such as SINDy with control [24], physics-informed SINDy [25–27], and a sparse structural system identification method applied to hysteretic systems [28] have significantly expanded its applicability to control systems, hidden-variable models, constrained physical systems, and hysteretic dynamics (our focus in this paper). Nevertheless, the effectiveness of SINDy-type methods strongly relies on the expressiveness of the chosen function library, which constrains their ability to capture non-polynomial dynamics, rate-dependent behaviors, and discontinuities. Selecting an appropriate function library is itself a nontrivial task, often requiring prior knowledge or trial-and-error tuning.

Even in extended variants such as weak SINDy [29] and implicit SINDy [30], sparse regression still primarily aims to identify governing equations from a prescribed candidate library, rather than directly reconstructing hysteretic trajectories. In hysteretic systems, many essential unobserved states are involved; in this paper, these are referred to as *hysteretic variables*. Unlike auxiliary hidden quantities in standard sparse regression settings, these variables are memory-dependent states that must be inferred consistently over time from the observed response to capture the system’s implicit evolution. This makes the identification problem fundamentally more challenging than standard hidden-state or implicit-form sparse regression, and consequently limits the suitability of these methods for hysteretic systems.

A variety of approaches have been proposed for equation discovery in hysteretic systems, which in this paper are classified according to the extent of prior knowledge assumed about the governing equations. In Figure 1, we organize the literature into four quadrants based on whether the structure of the primary dynamics equation ( $f_\theta$ ) and the hysteretic link equation ( $g_\phi$ ) are explicitly known or unknown. In the majority existing studies [28, 31], structural dynamics is assumed to follow an explicit known forms, while the hysteretic component is represented by an additional differential equation whose functional forms are to be discovered. Under this setting, the equation discovery task is reduced to symbolically identifying the hysteretic link equation (*Hysteresis Discovery* quadrant) [32, 33] or estimating parameters when structures of both equations are known (*Parameter Estimation* quadrant) [34–36]. Such assumptions greatly simplify the problem but restrict applicability to systems where the underlying structural model is already well characterized. On the other hand, frameworks that assume unknown

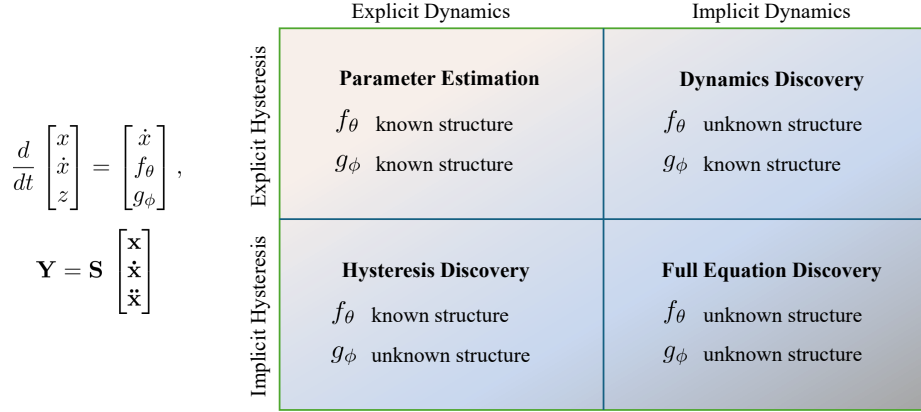


Figure 1: Classification of equation discovery approaches for hysteretic systems according to the assumed knowledge of the primary dynamics motion equation ( $f_\theta$ ) and the hysteretic link equation ( $g_\phi$ ). The displacement variable is represented by  $\mathbf{x} = [x(t_1), x(t_2), \dots, x(t_N)]^T$ , where  $N$  denotes the total number of sampled time points. The velocity variable  $\dot{\mathbf{x}}$  and acceleration variable  $\ddot{\mathbf{x}}$  are defined analogously. The selection matrix  $\mathbf{S} \in \mathbb{R}^{jN \times 3N}$  specifies which quantities are observed, where  $j = 1, 2$  or  $3$  is the number of available response components among displacement, velocity, and acceleration. Accordingly,  $\mathbf{Y} \in \mathbb{R}^{jN \times 1}$  denotes the corresponding available measurements. All these variables are dependent on  $t$ , which is omitted here for brevity. Each quadrant represents a level of prior structural specification.

structures in the primary dynamics equation (*Dynamics Discovery* quadrant) are far less common, particularly when hysteretic effects are present. When both the structural dynamics and the hysteretic link equations are unknown (*Full Equation Discovery* quadrant), the problem becomes substantially more challenging, requiring the simultaneous inference of two coupled, potentially nonlinear and memory-dependent governing equations.

It is noted that the above *Full Equation Discovery* setting is inherently less constrained than cases where part of the governing structure is known. The recovered symbolic forms and coefficients are commonly influenced by the operating regime and excitation levels represented in the training data, and identifiability is not fully guaranteed without sufficiently informative inputs and adequate sensing. Consequently, the physical interpretability of the explicitly recovered symbolic functional forms and coefficients, generalization to unseen excitation types or amplitude/frequency ranges, as well as robustness to measurement noise and modest parameter drifts, must be assessed rather than assumed. To the best of our knowledge, existing hysteresis equa-

tion discovery studies typically rely on partial structural assumptions (e.g., known primary dynamics or hysteretic link), and fully symbolic recovery of both the primary dynamics and hysteretic link in a coupled setting remains underexplored.

The above analysis highlights two major challenges in hysteretic systems: existing methods struggle to learn unobservable hysteretic variables when the hysteretic structure is entirely unknown, and library-based methods are limited in discovering governing equations with complex nonlinear expressions. In this research, we propose a unified framework that integrates hysteretic variable learning and symbolic regression (SR) to address the challenges of hysteretic equation discovery. The framework enables direct inference of hysteretic variables and recovery of explicit and interpretable governing equations without relying on predefined model libraries. Our contributions are as follows: (i) We provide a classification of equation discovery approaches for hysteretic systems and establish a unified framework that accommodates different levels of prior knowledge; (ii) We introduce a solver-based hysteretic variable learning scheme, where the state-space system is reformulated to enable inference of the trainable hysteretic variable, which is not directly measurable, and then combine it with SR to recover explicit governing equations from data without relying on a fixed predefined library; (iii) We validate the framework on synthetic benchmarks, a complex structure with high-order nonlinear and fractional terms, shake-table experiments, and a multiple degree-of-freedom (MDOF) system, demonstrating superior accuracy and generalizability compared with existing methods.

The remainder of this paper is organized as follows. Section 2 provides necessary preliminaries. Section 3 introduces the proposed methodology in detail. Section 4 presents numerical and experimental validation results. Section 5 concludes the paper with a summary of findings and directions for future research.

## 2. Preliminaries

### 2.1. Hysteretic models

In modeling hysteretic systems, hysteretic variables are commonly introduced to mathematically represent memory effects, history-dependent behavior, which allows the system’s response to account for past states.

Among hysteresis models, the Bouc-Wen model [7] is one of the most widely used, owing to its simplicity, and its capacity to represent a broad

range of hysteretic responses. It provides a set of differential equations to describe the evolution of hysteretic variables, and is capable of capturing both rate-dependent and asymmetric behaviors. The dynamics motion equation for a single degree-of-freedom (SDOF) nonlinear mass-spring-damper system with hysteresis can be expressed as follows:

$$m\ddot{x}(t) + c\dot{x}(t) + F(t) = u(t), \quad (1)$$

where  $x(t)$  is the displacement response;  $u(t)$  is the external excitation;  $m$  is the mass;  $c$  is the damping coefficient; and  $F(t)$  is the nonlinear restoring force that accounts for both elastic and hysteretic contributions. The restoring force is defined as:

$$F(t) = kx(t) + \alpha z(t), \quad (2)$$

where  $k$  is the stiffness,  $\alpha$  is the hysteretic coefficient, and  $z(t)$  is the hysteretic variable. Substituting Eq.(2) into Eq.(1), the equation of motion is rewritten as:

$$m\ddot{x}(t) + c\dot{x}(t) + kx(t) + \alpha z(t) = u(t). \quad (3)$$

Notably, setting  $\alpha = 0$  reduces the equation to classical linear behaviors.

The evolution of the hysteretic variable  $z(t)$  is governed by the Bouc-Wen hysteresis differential equation, which can also be written as an explicit function of  $\dot{x}(t)$  and  $z(t)$  for compactness and interpretability (for conciseness, we drop  $t$  in the equation):

$$\dot{z}(\dot{x}, z) = A\dot{x} - \beta|\dot{x}||z|^{n-1}z - \gamma\dot{x}|z|^n. \quad (4)$$

In this formulation, the parameter  $A$  serves as a linear amplification factor that scales the influence of the displacement rate on the evolution of the hysteretic variable. The coefficients  $\beta$  and  $\gamma$  jointly shape the energy dissipation and curvature of the hysteresis loop, with  $\beta$  primarily influencing the width and dissipation of the loop, while  $\gamma$  controls its nonlinear curvature. In most existing research [28, 33, 37], the exponent  $n$  is typically restricted to integer values. In practical Bouc-Wen modeling, however, allowing non-integer values of  $n$  provides a more flexible phenomenological parametrization for representing hysteretic loops with diverse transition smoothness and curvature that may not be adequately captured by integer exponents alone. In this research, we generalize the formulation by allowing  $n$  to take more general, including fractional values, thereby enabling richer characterization of various hysteresis.

## 2.2. Solvers of dynamic system

The governing equations of nonlinear dynamic systems are rarely solvable in closed form, and thus numerical integration schemes are commonly employed to approximate their time evolution. Classical approaches include implicit and explicit methods such as the Newmark- $\beta$  method, widely used in structural dynamics [38], linear multistep methods including Adams-Bashforth and Adams-Moulton schemes [39], and the family of Runge-Kutta algorithms [40]. Each solver provides a trade-off between accuracy, stability, and computational efficiency, and the choice of method is usually problem dependent.

For hysteretic models such as the Bouc-Wen formulation, the dynamics are described by a set of coupled nonlinear ordinary differential equations (ODEs) involving both the displacement response and an hysteretic variable. These equations can be integrated using standard time-stepping schemes, provided that sufficient resolution is maintained to capture the nonlinear hysteretic transition. In practice, explicit solvers are often favored for their simplicity and efficiency when the system stiffness is moderate.

Among these available options, the classical fourth-order Runge-Kutta (RK4) method is particularly attractive, offering a good balance between accuracy and computational cost. It is easy to implement and has been widely applied in physics and engineering for nonlinear system simulations. In this research, the RK4 scheme is embedded into the hysteretic variable learning process to integrate the hysteretic dynamics, yielding reliable reference trajectories that facilitate subsequent equation discovery.

## 2.3. Symbolic regression

Symbolic regression (SR) is a data-driven modeling approach that seeks to uncover the underlying mathematical relationships governing a system by simultaneously identifying both the model structure and its parameters [41]. Unlike conventional regression methods, SR does not assume a predefined functional form and focuses solely on parameter estimation. SR performs a global search over the space of possible mathematical expressions – typically represented as expression trees – to find the model that best fits the data. This search is guided by principles of accuracy, parsimony, and interpretability.

Mathematically, given a set of input-output data pairs  $\{(\mathbf{x}_i, y_i)\}_{i=1}^N$ , SR seeks to find an analytical function  $h(\cdot) \in \mathcal{H}$  such that:

$$y_i \approx h(\mathbf{x}_i; \delta), \quad \forall i = 1, \dots, N, \quad (5)$$

where  $\mathcal{H}$  denotes the space of candidate symbolic expressions constructed from a predefined set of mathematical operators (e.g.,  $+$ ,  $-$ ,  $\times$ ,  $\div$ ,  $\sin$ ,  $\cos \dots$ ), and  $\delta$  represents any tunable parameters involved in the expression. The optimal expression  $h^*$  is typically obtained by solving:

$$h^* = \arg \min_{h \in \mathcal{H}} (\mathcal{L}(h) + \lambda \Omega(h)), \quad (6)$$

where  $\mathcal{L}(h)$  is a loss function measuring the prediction error (e.g., mean squared error);  $\Omega(h)$  is a complexity penalty term (e.g., number of nodes in the expression tree); and  $\lambda$  is a regularization coefficient controlling the trade-off between accuracy and simplicity.

A feature of SR is its ability to discover explicit closed-form expressions without requiring prior specification of the model structure [42]. This property is particularly desirable in scientific discovery tasks where transparency and analytical interpretability are truly essential. Unlike black-box models such as neural networks, SR yields interpretable equations that can be directly analyzed, validated, or modified by domain experts. Recent algorithmic advances, including genetic programming, Monte Carlo tree search, and hybrid gradient-evolution strategies, have substantially improved both the computational efficiency and the overall expression quality of SR-generated models. Among these, notably, PySR [41] integrates evolutionary search with just-in-time compiled operators, thereby enabling scalable and efficient exploration of large expression spaces in scientific applications.

### 3. Methodology

#### 3.1. Problem definition and formulation

In this research, our objective is to output explicit differential equation representations of hysteretic systems, with both equation discovery and dynamic prediction. The proposed framework first introduces a state-space formulation:

$$\frac{d}{dt} \begin{bmatrix} x \\ \dot{x} \\ z \end{bmatrix} = \begin{bmatrix} \dot{x} \\ f_\theta(x, \dot{x}, u, z) \\ g_\phi \end{bmatrix}, \quad (7)$$

where  $x$  denotes the displacement, and  $\dot{x}$  is the velocity.  $f_\theta$  denotes the dynamic motion equation and  $g_\phi$  represents the hysteretic link equation. Our goal is to identify the explicit expressions of both  $f_\theta$  and  $g_\phi$ . The proposed unified framework is applicable to all four cases shown in Figure 1. Here,

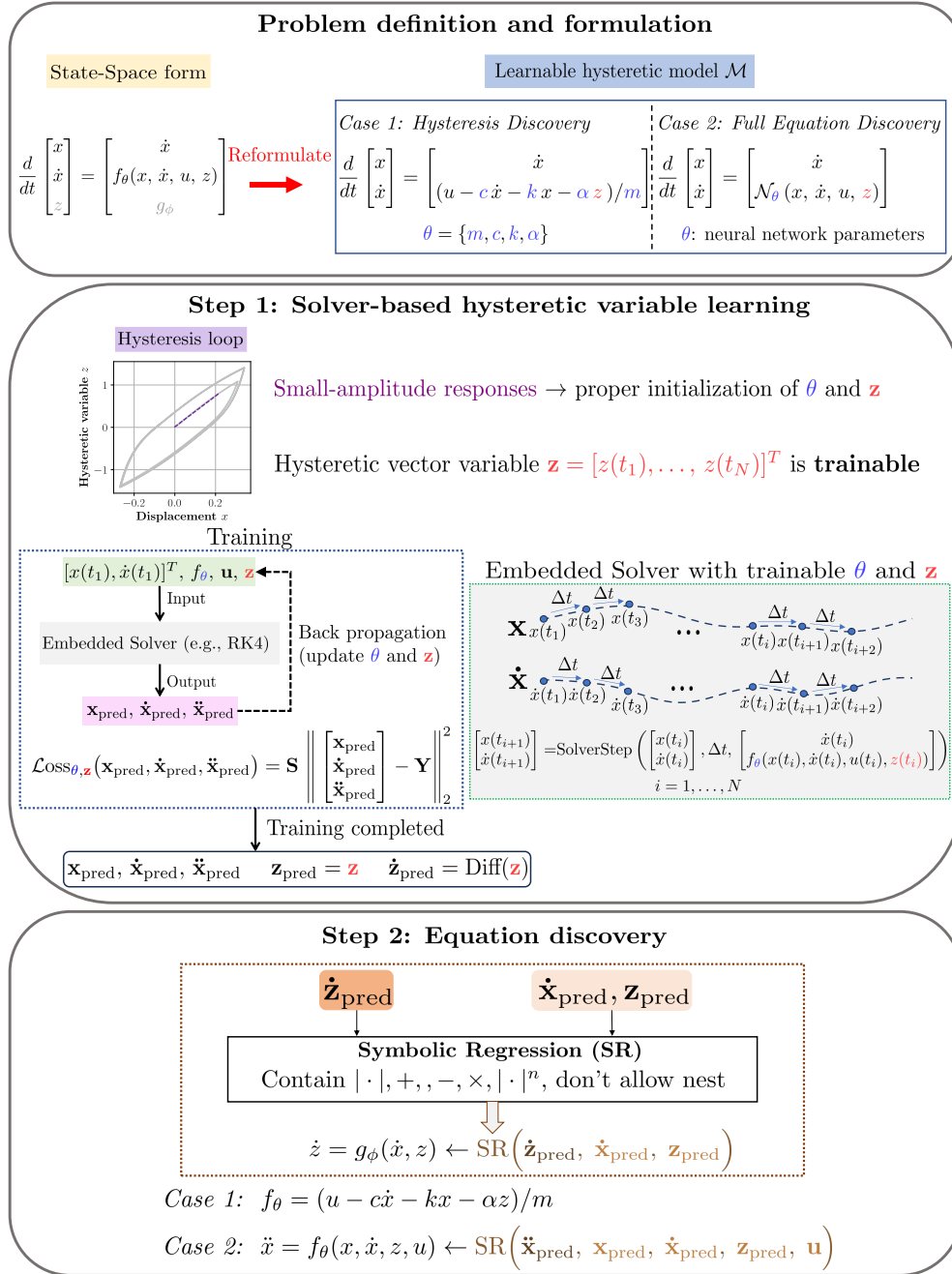


Figure 2: The proposed unified framework for equation discovery and dynamic prediction of hysteretic systems. **Problem definition and formulation:** The reformulated state-space form and learnable hysteretic model are established to describe the dynamic systems. Two cases in Figure 1 are considered as typical examples, where the hysteretic link equation ( $g_\phi$ ) is unknown. **Step 1:** The hysteretic vector variable  $\mathbf{z}$  is treated as trainable parameter. Small-amplitude responses are employed to proper initialization. A solver is embedded to update  $\theta$  and  $\mathbf{z}$  when back propagation, with the selection matrix  $\mathbf{S}$  (as in Figure 1) specifying the observed components in the loss function. **Step 2:** Symbolic regression (SR) extracts explicit and interpretable governing equations for both the dynamics motion equation ( $f_\theta$ ) (if Case 2) and hysteretic link equation ( $g_\phi$ ).

Table 1: Problem definition. Two cases of equation discovery approaches in Figure 1 for hysteretic systems.  $f_\theta$ : Dynamics motion equation.  $g_\phi$ : Hysteretic link equation.

Type	Case 1: <i>Hysteresis Discovery</i>	Case 2: <i>Full Equation Discovery</i>
Structure of $f_\theta$	Known (with unknown $m, c, k, \alpha$ )	Unknown
Structure of $g_\phi$	Unknown	
Expression of $f_\theta$	$f_\theta = (u - c\dot{x} - kx - \alpha z)/m$	$f_\theta = \mathcal{N}_\theta(x, \dot{x}, u, z)$
Expression of $\mathbf{z}$	Trainable vector variable	
Initialization of $m, c, k, \alpha$	Both <i>Case 1</i> and <i>Case 2</i> are required, estimated by $m\ddot{x}(t) + c\dot{x}(t) + kx(t) = u(t)$ using least-squares method, $\alpha$ is randomly initialized	
Initialization of $\theta$	$\theta = \{m, c, k, \alpha\}$ , initialized like above	$\theta$ : neural network parameters, randomly initialized
Initialization of $\mathbf{z}$	$z(t) = [u(t) - m\ddot{x}(t) - c\dot{x}(t) - kx(t)]/\alpha$	

we focus on two more complex cases in which  $g_\phi$  is unknown, namely, *Case 1: Hysteresis Discovery* and *Case 2: Full Equation Discovery*. The remaining two cases can be addressed using analogous procedures within the same framework. In particular, under the *Parameter Estimation* setting, where the structures of both  $f_\theta$  and  $g_\phi$  are known, our framework is only required to estimate the parameters, making it evidently a simpler case.

The differences and similarities between these two cases can be seen in Table 1. For both cases,  $g_\phi$  is assumed to be completely unknown. Therefore, we propose to reformulate the state-space system into a form that does not explicitly involve  $dz/dt$ :

$$\frac{d}{dt} \begin{bmatrix} x \\ \dot{x} \end{bmatrix} = \begin{bmatrix} \dot{x} \\ f_\theta(x, \dot{x}, u, z) \end{bmatrix}, \quad (8)$$

while  $z$  itself is treated as trainable thus still retained throughout the model.

The key distinction between these two cases lies in whether the structure of  $f_\theta$  is known. For *Case 1*, assuming that  $f_\theta$  is known as in Eq.(3), but the parameters in it are unknown. For *Case 2*, since the structure of  $f_\theta$  is also unknown, it is represented by a neural network  $\mathcal{N}_\theta(\cdot)$ , parameterized by trainable parameters  $\theta$ . More details on network architecture and training can be seen in Appendix A.

### 3.2. Solver-based hysteretic variable learning

Step 1 of the proposed framework focuses on solver-based hysteretic variable learning, in which the responses to the reformulated state-space are

simulated using an embedded numerical solver rather than via pointwise regression. Unlike pointwise regression methods that approximate the system’s temporal evolution at individual time steps, the solver-based approach enforces temporal consistency by integrating the governing equations over time, thereby capturing the implicit dependence of the hysteretic variable on the system states. This step is divided into following several parts.

**Trainable vector variable  $\mathbf{z}$ .** In both cases, the structure of the hysteretic link equation ( $g_\phi$ ) is unknown, and the hysteretic variable  $\mathbf{z}$  is unobserved. Therefore, we treat  $\mathbf{z}$  as a trainable hysteretic vector variable, which is optimized jointly with the model parameters  $\theta$ . This design is because  $g_\phi$  has a more complex expression, such as non-smooth operators, which is difficult to represent accurately with a neural network, whereas only the value of the vector  $\mathbf{z}$  is required in this step. Therefore, treating  $\mathbf{z}$  as a trainable parameter provides a more flexible and accurate formulation.

**Initialization.** To initialize the model parameters, small-amplitude responses are used to estimate the initial values of  $\theta$  and  $\mathbf{z}$ . Table 1 shows the initialization of two cases.

For *Case 1*,  $z(t)$  in Eq.(3) is omitted to simplify dynamic motion equation to:

$$m\ddot{x}(t) + c\dot{x}(t) + kx(t) = u(t). \quad (9)$$

Then, the initial values of  $m, c, k$  are estimated by the least-squares method, while the initial value  $\alpha$  is randomly initialized.

For *Case 2*, the parameters  $m, c, k, \alpha$  are obtained in the same way as in *Case 1* for estimating the initial value  $\mathbf{z}$ , and the neural network parameters  $\theta$  are randomly initialized.

For the initialization of  $\mathbf{z} = [z(t_1), z(t_2), \dots, z(t_N)]^T$ , where  $N$  denotes the total number of sampled time points, based on Eq.(3), we can express as:

$$z(t) = [u(t) - m\ddot{x}(t) - c\dot{x}(t) - kx(t)]/\alpha \quad (10)$$

and get the initial  $\mathbf{z}$ . This procedure provides a proper physically consistent initialization for the learnable hysteretic model, improving convergence and stability of solver-based optimization.

**Embedded Solver with trainable  $\theta$  and  $\mathbf{z}$ .** In this step, the governing equations are reformulated into a state-space representation, within which learnable hysteretic model is embedded inside a differentiable ODE solver such as RK4.

Given the known time stamps  $t_i$  ( $i = 1, 2, \dots, N$ ), the time step  $\Delta t$ , the corresponding input  $u_i$ , and the initial state  $[x(t_1), \dot{x}(t_1)]^T$ , the state trajectory can be computed sequentially using the ODE solver as:

$$\begin{bmatrix} x(t_{i+1}) \\ \dot{x}(t_{i+1}) \end{bmatrix} = \text{SolverStep} \left( \begin{bmatrix} x(t_i) \\ \dot{x}(t_i) \end{bmatrix}, \Delta t, \begin{bmatrix} \dot{x}(t_i) \\ f_\theta(x(t_i), \dot{x}(t_i), u(t_i), z(t_i)) \end{bmatrix} \right). \quad (11)$$

From above solver step, it can be seen that each element in the vector  $\mathbf{z} = [z(t_1), z(t_2), \dots, z(t_N)]^T$ , together with  $\theta$ , is used within the solver to generate the predicted responses  $\mathbf{x}_{\text{pred}}$ ,  $\dot{\mathbf{x}}_{\text{pred}}$ , and  $\ddot{\mathbf{x}}_{\text{pred}}$ , and is continuously updated during the training iterations. In this way, the solver is embedded into the subsequent training process.

**Training.** Based on the above embedded solver formulation, the training inputs are given by  $\{[x(t_1), \dot{x}(t_1)]^T, f_\theta, \mathbf{u}, \mathbf{z}\}$  ( $[x(t_1), \dot{x}(t_1)]^T$  is the initial condition), and the solver produces the predicted responses  $\mathbf{x}_{\text{pred}}$ ,  $\dot{\mathbf{x}}_{\text{pred}}$ , and  $\ddot{\mathbf{x}}_{\text{pred}}$ . In both cases, training is performed by backpropagation to update the parameters  $\theta$  and  $\mathbf{z}$ .

We design a loss function that is flexible to the types of available data. Given the known time stamps  $t_i, i = 1, 2, \dots, N$ , the corresponding system responses such as  $x(t_i)$ ,  $\dot{x}(t_i)$ , and  $\ddot{x}(t_i)$  (which may include a subset of them depending on sensing). As shown in Figures 1 and 2, the formulation is flexible with respect to the available system responses. The corresponding loss function is:

$$\mathcal{L}_{\text{OSS}_{\theta, \mathbf{z}}}(\mathbf{x}_{\text{pred}}, \dot{\mathbf{x}}_{\text{pred}}, \ddot{\mathbf{x}}_{\text{pred}}) = \left\| \mathbf{S} \begin{bmatrix} \mathbf{x}_{\text{pred}} \\ \dot{\mathbf{x}}_{\text{pred}} \\ \ddot{\mathbf{x}}_{\text{pred}} \end{bmatrix} - \mathbf{Y} \right\|_2^2, \quad (12)$$

where the selection matrix  $\mathbf{S}$  specifies which quantities are observed and  $\mathbf{Y}$  denotes the corresponding available measurements (the same definitions as Figure 1).

In practice, when some response components are not directly measured, they can be reconstructed from the available signals through smoothing, numerical differentiation, or numerical integration. In our examples, this means that the full set of responses is numerically completed, so that  $\mathbf{S}$  is an identity matrix. More generally, in our framework,  $\mathbf{S}$  can be specified flexibly according to the available observations, because  $x(t_i)$ ,  $\dot{x}(t_i)$ , and  $\ddot{x}(t_i)$  can all be incorporated into the optimization of  $\theta$  and  $\mathbf{z}$ . This is one aspect of the flexibility of the proposed framework.

Once training is completed, the predicted system responses  $\mathbf{x}_{\text{pred}}$ ,  $\dot{\mathbf{x}}_{\text{pred}}$ , and  $\ddot{\mathbf{x}}_{\text{pred}}$ , together with the predicted hysteretic variable  $\mathbf{z}_{\text{pred}}$ , are obtained. The corresponding  $\dot{\mathbf{z}}_{\text{pred}}$  is then computed via finite differences, denoted  $\text{Diff}(\mathbf{z}_{\text{pred}})$ .

Through this step, the hysteretic variable is learned directly from measurements, addressing one of the central difficulties in hysteresis modeling. Importantly, this process avoids restrictive assumptions, such as prescribing a specific functional form for the hysteretic link equation ( $g_\phi$ ) or relying on strongly constrained structural priors, and provides essential data-driven guidance for the subsequent Step 2: Equation discovery, where SR is employed to recover explicit governing equations.

### 3.3. Equation discovery

Step 2 of the framework is dedicated to extracting interpretable governing equations. For the hysteretic link equation ( $g_\phi$ ), as illustrated in Figure 2, symbolic regression (SR) is applied to the learned trajectories of  $\dot{x}_{\text{pred}}$ ,  $z_{\text{pred}}$ , and  $\dot{z}_{\text{pred}}$  to search for mathematical expressions  $\dot{z} = g_\phi(\dot{x}, z)$ , and this can be written as  $\text{SR}(\dot{z}_{\text{pred}}, \dot{x}_{\text{pred}}, z_{\text{pred}})$ . For dynamic motion equation ( $f_\theta$ ), in *Case 1: Hysteresis Discovery*, with known equation structure and the estimated values of  $m, c, k, \alpha$ , the discovered dynamic motion equation is expressed as  $f_\theta = (u - c\dot{x} - kx - \alpha z)/m$ ; in *Case 2: Full Equation Discovery*, using the same SR method like  $g_\phi$ , we can obtain the discovered dynamic motion equation  $\ddot{x} = f_\theta(x, \dot{x}, z, u)$ , and this can be written as  $\text{SR}(\ddot{x}_{\text{pred}}, x_{\text{pred}}, \dot{x}_{\text{pred}}, z_{\text{pred}}, u)$ .

A key advantage of SR lies in its flexibility. Unlike approaches such as SINDy that rely on a predefined functional library, SR enables customization of the search space by incorporating possible operators (e.g., absolute value and exponential) and explicit control over expression complexity. In particular, SR allows the specification of operator forms without fixing their exact exponents or coefficients – for example, one can include  $|\cdot|^n$  with  $n$  treated as a free constant to be learned. This stands in contrast to SINDy, which requires enumerating many such candidate terms in the predefined library, making it impractical or unfriendly when  $n$  is non-integer. Our subsequent experiments will further illustrate this difference. This adaptability mitigates overfitting, promotes interpretability, and facilitates the recovery of compact, physically plausible differential equations that reliably describe the system dynamics. We also acknowledge that SR introduces a mild structural prior through its user-specified operator set and search constraints. In this work, we use a compact operator set  $\{+, -, \times, |\cdot|, |\cdot|^n\}$  (with  $n$

identified as a free constant) together with an explicit complexity penalty and simple grammar constraints (e.g., excluding division and disallowing nested absolute/absolute-power compositions) to promote parsimony and reproducibility, which defines the admissible space of discoverable equations. Additional details on the computational complexity and scalability of the proposed framework are given in Appendix A.

#### 4. Experiments

To evaluate the effectiveness and robustness of the proposed framework, we apply the framework to a series of experiments on representative hysteretic systems. These experiments aim to assess both predictive accuracy and generalization ability under varying excitation types, noise conditions and initial conditions. For the noise conditions part, robustness with respect to measurement uncertainty is examined by adding zero-mean Gaussian white noise to the measured data, with signal-to-noise ratio (SNR) defined as:

$$\text{SNR}(\text{dB}) = 10 \log_{10} \left( \frac{P_{\text{signal}}}{P_{\text{noise}}} \right), \quad (13)$$

where  $P_{\text{signal}}$  and  $P_{\text{noise}}$  denote the average power of the clean signal and the added noise, respectively. To better demonstrate the performance of the proposed framework, the prediction accuracy is quantified using the normalized root mean square error (NRMSE), defined as:

$$\text{NRMSE}(y_{\text{pred}}, y_{\text{true}}) = \frac{\sqrt{\frac{1}{N} \sum_{i=1}^N (y_{\text{pred},i} - y_{\text{true},i})^2}}{\max\{y_{\text{true}}\} - \min\{y_{\text{true}}\}}, \quad (14)$$

where  $y_{\text{true},i}$  and  $y_{\text{pred},i}$  denote the  $i$ -th observed (ground truth) and predicted values of the target quantity, respectively;  $N$  is the total number of samples. The normalization by the range of  $y_{\text{true}}$  ensures scale-invariant comparison across different datasets or measurement magnitudes.

The subsequent subsections present four case studies of increasing complexity: (i) the Bouc-Wen hysteretic system benchmark, (ii) a complex structure with nonlinear and fractional terms, (iii) an experimental single degree-of-freedom (SDOF) yielding structure, and (iv) Extension to multiple degree-of-freedom (MDOF) systems. Collectively, these experiments provide a comprehensive evaluation of the proposed framework.

#### 4.1. Bouc-Wen hysteretic system benchmark

The Bouc-Wen hysteretic benchmark, developed by Noël and Schoukens [43], provides a well-established testbed for evaluating nonlinear system identification methods under hysteretic dynamics. The benchmark builds on the Bouc-Wen model of hysteresis [7, 44], which has been extensively used in structural dynamics and control applications [45, 46]. The benchmark data are generated through accurate integration of the Bouc-Wen equations using a Newmark scheme, including estimation data obtained from noisy multisine excitations for model identification, as well as separate fixed test datasets for validation. In particular, two fixed test datasets are provided: (i) a sinesweep excitation with amplitude of 40 N sweeping from 20 - 50 Hz and (ii) a random-phase multisine excitation covering the 5 - 150 Hz frequency band [43]. These datasets are widely adopted in the system identification community for assessing generalization capabilities of nonlinear models.

In our experiments, the sinesweep dataset is used for training, while the multisine dataset is reserved for testing. This configuration evaluates the ability of the proposed framework to generalize across different excitation types. The goal is not only to capture the nonlinear hysteretic dynamics present in the training data but also to validate robustness and predictive accuracy under unseen forcing conditions.

The Bouc-Wen hysteretic system can be described by a SDOF nonlinear mass-spring-damper oscillator, where the restoring force includes both elastic and hysteretic components. Following the benchmark description in [43], the dynamics are governed by the coupled differential equations:

$$\begin{cases} m\ddot{x}(t) + c\dot{x}(t) + kx(t) + \alpha z(t) = u(t), \\ \dot{z}(t) = A\dot{x}(t) - \beta|\dot{x}(t)||z(t)|^{n-1}z(t) - \gamma\dot{x}(t)|z(t)|^n, \end{cases} \quad (15)$$

where  $x(t)$  is the displacement response,  $u(t)$  is the external excitation, and  $z(t)$  is the hysteretic variable. The parameters  $m$ ,  $c$ , and  $k$  denote the mass, damping, and linear stiffness, respectively, while  $\alpha$ ,  $A$ ,  $\beta$ ,  $\gamma$ , and  $n$  control the amplitude, shape, and smoothness of the hysteresis loop. For the benchmark configuration, the parameters are set to  $m = 2.0$ ,  $c = 10.0$ ,  $k = 50000.0$ ,  $\alpha = 1.0$ ,  $A = 50000.0$ ,  $\beta = 800.0$ ,  $\gamma = -1100.0$  and  $n = 1.0$ .

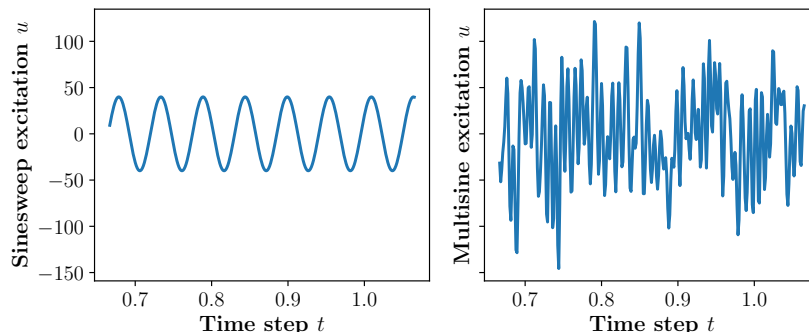


Figure 3: Different types of external excitation of benchmark data. The sinesweep signal (left) is used as the training input (Training and Testing 1), while the multisine signal (right) serves as the testing input (Testing 2).

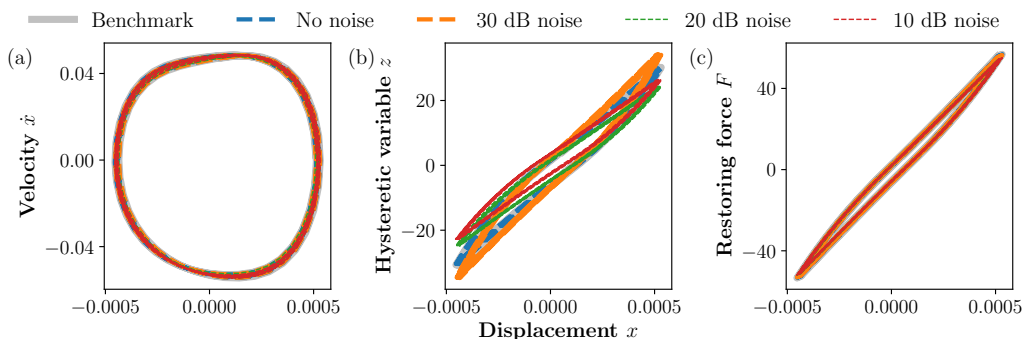


Figure 4: Hysteresis loops of benchmark data. (a)  $x - \dot{x}$  hysteresis loop. (b)  $x - z$  hysteresis loop. (c)  $x - F (F = kx + \alpha z)$  hysteresis loop.

As the first benchmark case, Figure 3 illustrates the two external excitations employed for sinesweep signal training and multisine signal testing. In addition, we further consider noisy scenarios by adding Gaussian noise with signal-to-noise ratios of 30 dB, 20 dB, and 10 dB, corresponding to low, medium, and high noise levels, respectively.

In our framework, the structure of the hysteretic link equation  $\dot{z} = g_\phi(\dot{x}, z)$  is regarded as unknown in both *Case 1: Hysteresis Discovery* and *Case 2: Full Equation Discovery*. In this experiment, this means that the second equation in Eq. (15) is not assumed a priori. Accordingly, the subsequent results are reported as “discovered equations”, rather than merely “parameter estimation”. We do not prescribe a classical or generalized Bouc-Wen

functional form for the hysteretic evolution. Instead, the hysteretic variable trajectory is first learned through the solver-based scheme, and symbolic regression (SR) is then used to recover an explicit symbolic expression for the hysteretic link. Here, we assume to know the structure of the dynamics motion equation, thus it is a problem of *Hysteresis Discovery*. Figure 4 shows the hysteresis loops learned by the proposed framework, in terms of three different representations. It can be observed that, even in the presence of strong noise, the proposed model successfully captures nonlinear memory-dependent hysteretic behaviors.

We define two different types of testing cases. In Testing 1, the external excitation is the same as in Training, but the data are taken from a time span beyond the training window. In Testing 2, an unseen external excitation is applied, providing an out-of-distribution scenario relative to training.

For a quantitative evaluation, Tables 2 and 3 report the performance in terms of discovered equations and NRMSE at different noise levels, respectively. The results show that the proposed framework consistently achieves an accurate reconstruction of explicit governing equations, with the responses reproduced from the discovered explicit equations exhibiting low NRMSE values.

To further evaluate the validity of the discovered models, the displacement and velocity responses obtained by numerically solving the discovered governing equations are compared with the corresponding ground truth results in Figures 5 and 6, respectively. This procedure more directly high-

Table 2: Discovered equations results of benchmark data ( $t$  is omitted for brevity).

<b>True equations</b>	$2.0000\ddot{x} + 10.0000\dot{x} + 50000.0000x + 1.0000z = u$ $\dot{z} = 50000.0000\dot{x} - 800.0000 \dot{x} z + 1100.0000\dot{x} z $
<b>Noise</b>	<b>Discovered equations</b>
Noise-free	$1.9998\ddot{x} + 10.0231\dot{x} + 49893.8617x + 1.0110z = u$ $\dot{z} = 49633.1496\dot{x} - 779.1857 \dot{x} z + 1049.3318\dot{x} z $
30dB	$1.8623\ddot{x} + 10.2269\dot{x} + 47507.9528x + 1.0210z = u$ $\dot{z} = 50858.0627\dot{x} - 734.82275 \dot{x} z + 922.7398\dot{x} z $
20dB	$1.7976\ddot{x} + 12.8240\dot{x} + 46127.6819x + 1.2557z = u$ $\dot{z} = 43574.2517\dot{x} - 727.0708 \dot{x} z + 727.0708\dot{x} z $
10dB	$1.6149\ddot{x} + 14.8180\dot{x} + 45758.4897x + 1.4018z = u$ $\dot{z} = 402647.4894\dot{x} - 700.5687 \dot{x} z + 700.5687\dot{x} z $

Table 3: NRMSE results of benchmark data.

Noise	Responses	Training NRMSE	Testing 1 NRMSE	Testing 2 NRMSE
Noise-free	Displacement $x$	0.15%	0.13%	0.93%
	Velocity $\dot{x}$	0.44%	0.49%	1.06%
30 dB	Displacement $x$	0.85%	0.78%	0.67%
	Velocity $\dot{x}$	1.29%	1.13%	0.96%
20 dB	Displacement $x$	2.41%	1.64%	3.30%
	Velocity $\dot{x}$	3.08%	2.15%	3.37%
10 dB	Displacement $x$	4.80%	4.52%	5.11%
	Velocity $\dot{x}$	5.57%	5.90%	6.13%

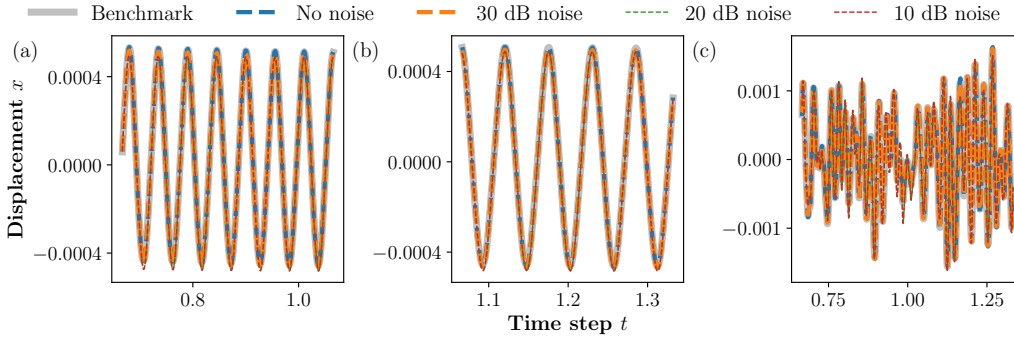


Figure 5: Displacement results of benchmark data. (a) Training results. (b) Testing 1 (same excitation) results. (c) Testing 2 (unseen excitation) results.

lights the effectiveness of equation discovery. This benchmark experiment demonstrates that the unified framework is capable of reliably identifying hysteretic dynamics, even under noisy conditions. These findings validate the effectiveness of the proposed methodology for equation discovery and dynamic prediction of nonlinear hysteretic systems.

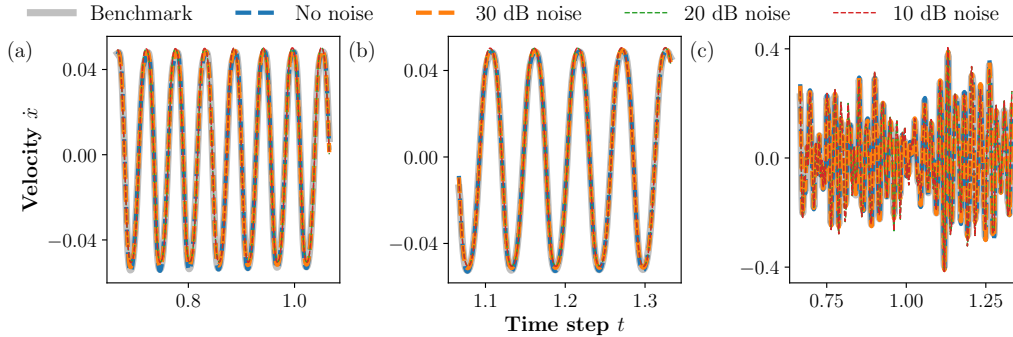


Figure 6: Velocity results of benchmark data. (a) Training results. (b) Testing 1 (same excitation) results. (c) Testing 2 (unseen excitation) results.

To further validate the proposed framework, we also conduct some additional benchmark experiments beyond the baseline setting: *Cross-excitation validation*, *Extrapolation test on unseen amplified excitation*, *Sensitivity analyses*, *Noisy wideband random excitation training* and *Without hysteresis*. The detailed context can be seen in Appendix C.

#### 4.2. A complex structure with high-order nonlinear and fractional terms

The second experiment considers a more complex hysteretic system to further evaluate the flexibility of the proposed framework. In this case, the restoring force incorporates a cubic nonlinearity in the displacement response, and the hysteretic evolution equation involves a fractional exponent  $n$ , thereby introducing additional challenges compared to the standard Bouc-Wen formulation. The governing equations are given by:

$$\begin{cases} m\ddot{x}(t) + c\dot{x}(t) + kx(t)^3 + \alpha z(t) = u(t), \\ \dot{z}(t) = A\dot{x}(t) - \beta|\dot{x}(t)||z(t)|^{n-1}z(t) - \gamma\dot{x}(t)|z(t)|^n, \end{cases} \quad (16)$$

with system parameters  $m = 1.0$ ,  $c = 0.8$ ,  $k = 0.5$ ,  $\alpha = 1.0$ ,  $A = 4.0$ ,  $\beta = 5.0$ , and  $\gamma = -4.0$ . Unlike the benchmark case, here we let  $n = 1.5$  (fractional), which modifies the smoothness and sharpness of the hysteretic transition and better reflects diverse hysteretic behaviors.

This experiment highlights the unified nature of the framework, as it remains applicable even when the underlying system exhibits higher-order nonlinearities and non-integer hysteretic exponents. In this experiment, we consider the two cases: *Hysteresis Discovery* and *Full Equation Discovery*.

Before presenting the main experimental results, we first examine the sensitivity of the learned hysteretic variable to initialization in the most challenging *Full Equation Discovery* setting in this experiment. Specifically, we consider a fixed training case with only one initial condition and one excitation, while initializing the trainable hysteretic variable  $\mathbf{z}$  through Step 1 in three different strategies: (a) Ours: initialization described in Section 3.2, (b) Zero:  $z(t) = 0$ , (c) Sine:  $z(t) = \sin(2\pi t)$ . Figure 7 shows the  $x$ - $z$  hysteresis loops for these three strategies at initialization and after convergence. Figure 8 shows the Step 1 predicted results, it can be seen that all three initialization strategies can accurately predict  $x$ ,  $\dot{x}$ , and  $\ddot{x}$ .

However, the strategies Zero and Sine struggle to recover the correct hysteresis loops, indicating that accurate response prediction does not necessarily imply accurate learning of the hysteretic variable. Although the initial hysteresis loop delivered by our initialization strategy differs from the ground truth, it captures hysteretic features compared with the other two strategies. After training, the final optimized results become much closer to the ground truth.

This result suggests that, when the training data are not sufficiently informative, strict uniqueness of the learned hysteretic variable cannot be asserted. Nevertheless, the proposed solver-based learning scheme remains a practically effective initialization strategy. This example represents a relatively extreme case, as only a single training trajectory is used. It also highlights the importance of sufficient diversity in the training data, which is examined in this experiment by considering multiple initial conditions.

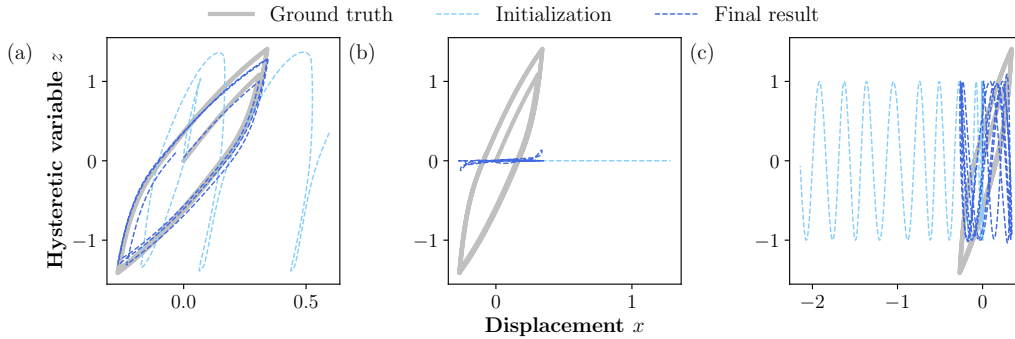


Figure 7:  $x$ - $z$  hysteresis loops under the same single initial condition and excitation in the *Full Equation Discovery* setting of complex structure data. Three different strategies: (a) Ours: initialization described in Section 3.2. (b) Zero:  $z(t) = 0$ . (c) Sine:  $z(t) = \sin(2\pi t)$ .

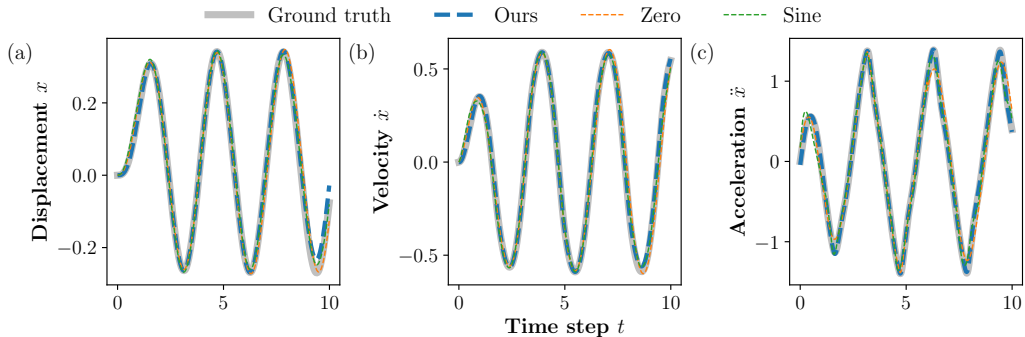


Figure 8: Predicted response results in Step 1 of complex structure data. (a) Displacement results. (b) Velocity results. (c) Acceleration results.

In this experiment, the training data are generated from five different initial conditions, while an additional unseen initial condition is used for testing to evaluate the generalizability of the proposed framework. The external excitation is defined as  $u(t) = \sin(2t)$ , representing a smooth periodic input suitable for a dynamic system. The sampling frequency is set to  $f_s = 100$  Hz, and the total simulation duration is  $T = 6$  s. Such a setup allows for a comprehensive assessment of the model’s robustness under varying initial states while maintaining consistent excitation characteristics.

To compare the proposed framework with a representative sparse regression pipeline, we use SINDy [24], which discovers governing equations by performing sparse regression over a pre-defined candidate function library. In addition to the vanilla SINDy, we include two advanced SINDy methods to provide a fairer comparison under strong nonlinearity and noisy measurements. Specifically, we consider parallel implicit SINDy (SINDy-PI) [30], which identifies implicitly defined governing relations and leverages multiple trajectories to improve identifiability, and Weak SINDy [29], which performs identification in an integral (weak) form to reduce sensitivity to derivative noise. For all SINDy-based methods, we use a candidate library design that is made as consistent as possible with our method, and we tune the key sparsity-related hyperparameters on the training set to avoid biasing the comparison. Specifically, the dynamic motion equation is assumed to be a linear combination of  $x$ ,  $\dot{x}$ ,  $z$ , and  $u$ , whereas the hysteretic link equation is constrained to include absolute-value terms and their integer powers from 1 to 5, thereby providing SINDy with sufficient expressive capacity to capture nonlinear hysteretic behaviors.

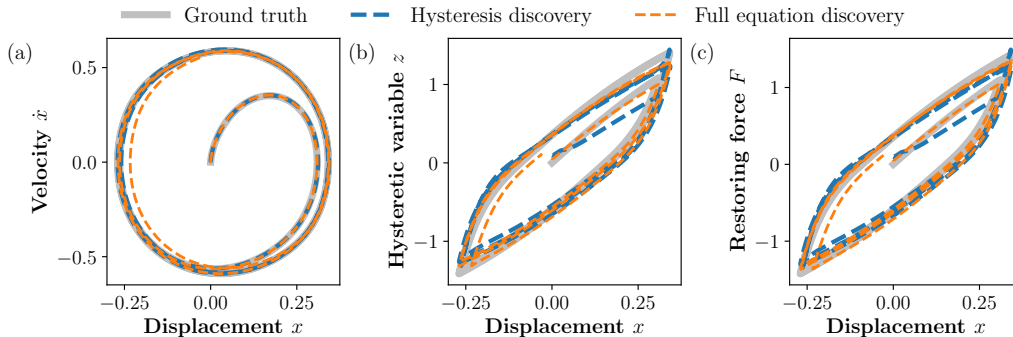


Figure 9: Hysteresis loops of complex structure data. (a)  $x - \dot{x}$  hysteresis loop. (b)  $x - z$  hysteresis loop. (c)  $x - F (F = kx^3 + \alpha z)$  hysteresis loop.

Figure 9 shows the hysteresis loops learned by the proposed framework. Both configurations can capture qualitative hysteretic behavior, yet the *Hysteresis Discovery* model clearly achieves better accuracy in reconstructing the loop dynamics. Table 4 lists the explicit forms of the discovered equations, and Table 5 reports the NRMSE results for all methods. It can be seen that Weak SINDy improves the response-level accuracy over vanilla SINDy, most notably under *Hysteresis Discovery*, whereas SINDy-PI provides limited gains and becomes less reliable in *Full Equation Discovery*, where the recovered dynamics can deviate substantially from the true responses.

Figures 10 and 11 compare the displacement, velocity, and acceleration responses obtained by solving the discovered equations, compared with the corresponding ground truth responses in the training and testing datasets, respectively. Despite the partial improvement brought by Weak SINDy, both SINDy-PI and Weak SINDy remain constrained by the predefined integer-order candidate library and therefore fail to recover the fractional-order hysteretic terms. As shown in Table 4, they tend to introduce spurious integer-power terms as compensation. By contrast, our method consistently identifies fractional exponents close to the ground truth and achieves the lowest errors in both training and testing (Table 5), with *Hysteresis Discovery* remaining more accurate than *Full Equation Discovery* due to the benefit of incorporating prior structural knowledge of dynamics motion equation ( $f_\theta$ ).

From these results, it is evident that the proposed framework consistently outperforms SINDy-based methods, achieving lower errors and more faithful recovery of the governing equations. A notable difference is that,

Table 4: Discovered equations results of complex structure data ( $t$  is omitted for brevity). SINDy fails to recover the fractional-order terms and instead introduces spurious integer-order terms to compensate.

<b>True equations</b>	$1.0000\ddot{x} + 0.8000\dot{x} + 0.5000x^3 + 1.0000z = 1.0000u$ $\dot{z} = 4.0000\dot{x} - 5.0000 \dot{x}  z ^{0.5}z + 4.0000\dot{x} z ^{1.5}$
<b>Type and method</b>	<b>Discovered equations</b>
<b><i>Hysteresis Discovery</i> (Ours)</b>	<b><math>0.9388\ddot{x} + 0.7934\dot{x} + 0.5366x^3 + 1.0320z = u</math></b> <b><math>\dot{z} = 4.0633\dot{x} - 4.8310 \dot{x}  z ^{0.5486}z + 3.8942\dot{x} z ^{1.5486}</math></b>
<i>Hysteresis Discovery</i> (SINDy)	$\ddot{x} + 0.8445\dot{x} + 0.5679x^3 + 1.0992z = 1.0649u$ $\dot{z} = -6.80922 \dot{x}  z z + 5.00018 \dot{x}  z ^2z + 4.98652\dot{x} z ^2 + 3.73699\dot{x}$
<i>Hysteresis Discovery</i> (SINDy-PI)	$0.9097\ddot{x} + 0.7685\dot{x} + 0.5165x^3 + 1.0000z = 0.9689u$ $\dot{z} = - \dot{x}  z ^2z + 0.4263 \dot{x}  z z - 0.0583 \dot{x} z + 0.0258\dot{x} z ^2$
<i>Hysteresis Discovery</i> (Weak SINDy)	$\ddot{x} + 0.8483\dot{x} + 0.5715x^3 + 1.1007z = 1.0678u$ $\dot{z} = 17.7907\dot{x} z ^2 - 6.4668 \dot{x}  z z + 3.9354\dot{x} - 1.9870 \dot{x} z$
<b><i>Full Equation Discovery</i> (Ours)</b>	<b><math>\ddot{x} + 0.7689\dot{x} + 0.4573x^3 + 1.0423z = 0.9503u</math></b> <b><math>\dot{z} = 4.0543\dot{x} - 5.1348 \dot{x}  z ^{0.6225}z + 3.8224\dot{x} z ^{1.6225}</math></b>
<i>Full Equation Discovery</i> (SINDy)	$\ddot{x} + 0.7490\dot{x} + 0.5833x^3 + 1.2145z = 0.8992u$ $\dot{z} = -12.704 \dot{x}  z z + 6.118 \dot{x}  z ^2z + 2.941\dot{x} z ^2 - 0.873\dot{x}$
<i>Full Equation Discovery</i> (SINDy-PI)	$0.0330\ddot{x} + 0.0601\dot{x} + x^3 + 0.0555z = 0.0082u$ $\dot{z} = - \dot{x}  z ^2z + 0.4346 \dot{x}  z z - 0.0602 \dot{x} z - 0.0108\dot{x} z ^2$
<i>Full Equation Discovery</i> (Weak SINDy)	$\ddot{x} + 0.0826\dot{x} + 0.84054x^3 + 1.2282z = 0.6778u$ $\dot{z} = -2.6871 \dot{x}  z z + 5.5021\dot{x} z  - 3.6203\dot{x} z ^2 + 3.2106\dot{x}$

unlike SR, SINDy cannot flexibly capture fractional exponents. Compared with the vanilla SINDy, SINDy-PI and Weak SINDy partially improve the response-level accuracy, especially in the *Hysteresis Discovery* setting. In our framework, both *Hysteresis Discovery* and *Full Equation Discovery* can successfully recover expressions with fractional exponents, which is generally beyond the capability of library-based approaches such as SINDy. By contrast, the *Full Equation Discovery* setting—where both the dynamics motion equation and the hysteretic link equation are unknown—yields slightly lower accuracy than *Hysteresis Discovery*. In practice, it is suggested that incorporating some prior knowledge helps improve accuracy and equation discovery performance.

Table 5: NRMSE results of complex structure data.

Type	Responses	Method	Training NRMSE	Testing NRMSE
<i>Hysteresis Discovery</i>	Displacement $x$	<b>Ours</b>	<b>4.21%</b>	<b>3.84%</b>
		SINDy	25.42%	36.87%
		SINDy-PI	25.48%	28.37%
		Weak SINDy	7.77%	10.19%
	Velocity $\dot{x}$	<b>Ours</b>	<b>3.91%</b>	<b>4.01%</b>
		SINDy	24.79%	39.50%
		SINDy-PI	20.56%	26.73%
		Weak SINDy	8.03%	12.06%
	Acceleration $\ddot{x}$	<b>Ours</b>	<b>3.86%</b>	<b>3.88%</b>
		SINDy	25.70%	40.67%
		SINDy-PI	20.07%	27.66%
		Weak SINDy	7.79%	12.43%
<i>Full Equation Discovery</i>	Displacement $x$	<b>Ours</b>	<b>5.28%</b>	<b>4.57%</b>
		SINDy	25.73%	37.76%
		SINDy-PI	22.92%	41.41%
		Weak SINDy	15.82%	21.68%
	Velocity $\dot{x}$	<b>Ours</b>	<b>4.56%</b>	<b>4.25%</b>
		SINDy	26.56%	32.43%
		SINDy-PI	21.97%	37.71%
		Weak SINDy	18.86%	20.55%
	Acceleration $\ddot{x}$	<b>Ours</b>	<b>4.86%</b>	<b>4.31%</b>
		SINDy	23.00%	36.15%
		SINDy-PI	22.02%	32.64%
		Weak SINDy	17.24%	20.80%

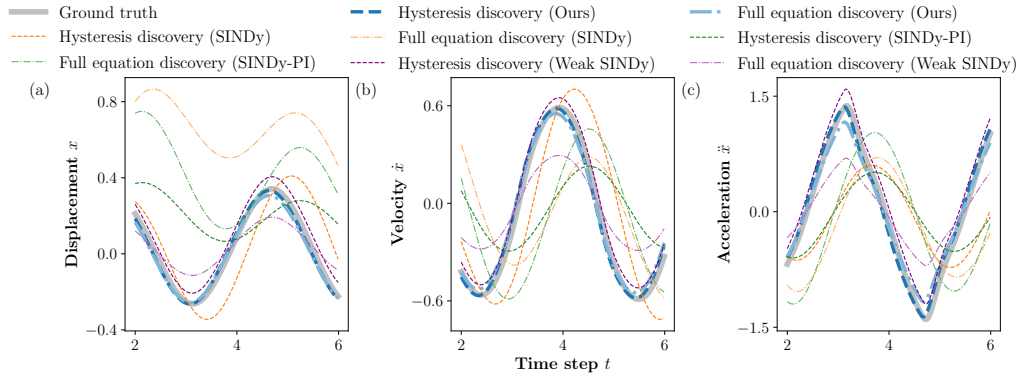


Figure 10: Training results of complex structure data. (a) Displacement results. (b) Velocity results. (c) Acceleration results.

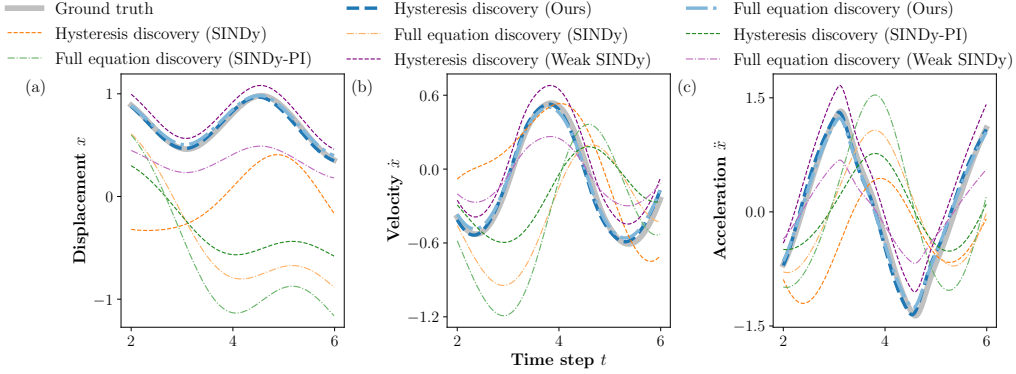


Figure 11: Testing results of complex structure data. (a) Displacement results. (b) Velocity results. (c) Acceleration results.

#### 4.3. An experimental SDOF yielding structure

In this experiment, a shear-type SDOF yielding structure excited by shake-table ground motions is implemented to investigate the proposed framework method. The experimental setup of the braced 3-story structure (equivalent to a SDOF system), with and without a negative stiffness device (NSD) [47, 48] is illustrated in Figure 12 [28, 49, 50], where the NSD is installed on the first floor to alter hysteretic behaviors.

We adopt the governing equation structure  $m\ddot{x}(t) + c\dot{x}(t) + kx(t) + \alpha z(t) = -mu(t)$ , where  $x(t)$  is the displacement,  $\dot{x}(t)$  and  $\ddot{x}(t)$  are its velocity and acceleration,  $u(t)$  is the measured base acceleration, and  $z(t)$  is the hysteretic variable. This setup belongs to the *hysteresis discovery* type, in which the structure of the equation of motion is predefined (which needs to identify unknown system parameters), and the nonlinear hysteretic link equation is assumed to be unknown.

We reuse the real shake table experiment from [28], and study the structure in two scenarios: (i) *without* an NSD and (ii) *with* an NSD installed on the first floor. Following the setup in [28], we use the measured displacement  $x(t)$ , the computed velocity  $\dot{x}(t)$  (via differentiation and smoothing), the measured acceleration  $\ddot{x}(t)$ , and the shake-table excitation  $u(t)$  as inputs to our framework. For the *without NSD* case, a type-I 60% scaled Pacoima earthquake is used for training, and a reversed type-II 60% Pacoima record for testing. For the *with NSD* case, the training signal concatenates 43% and 65% scaled Pacoima segments, while the testing input is a 55% scaled Sylmar record (see Figs 23–25 of [28] for details).

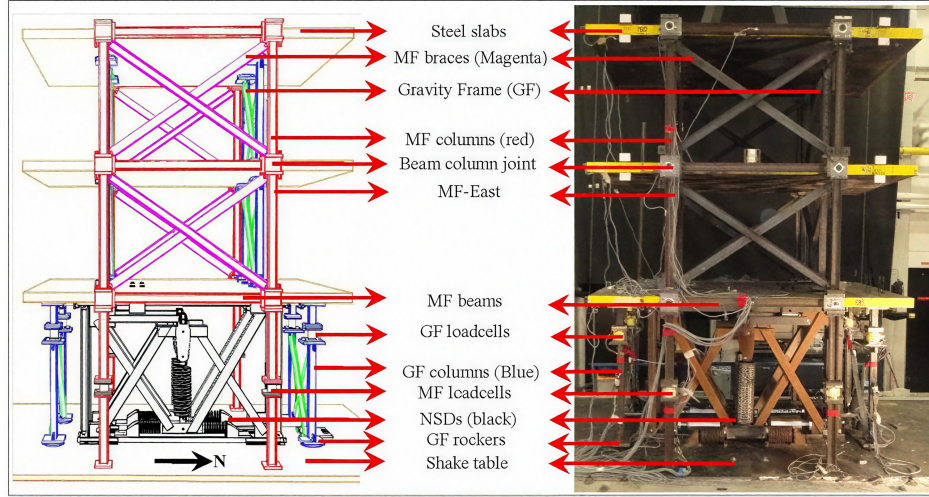


Figure 12: Shaking table test of a braced 3-story structure (equivalent to a SDOF system), with a negative stiffness device (NSD) installed on the first floor [28].

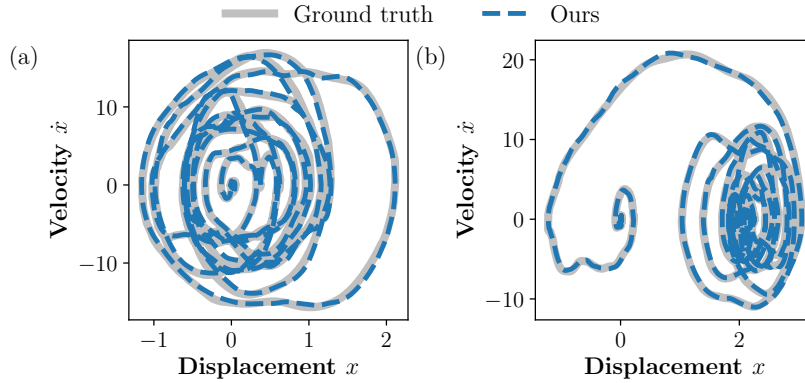


Figure 13:  $x - \dot{x}$  hysteresis loops of yielding structure. (a) Without NSD. (b) With NSD.

For the *without NSD* case, the hysteresis loop in the  $x - \dot{x}$  plane is presented in Figure 13 (a). The discovered evolution law reduces to a rate-dominated form  $\dot{z}(t) = 2.1847\dot{x}(t)$ , together with the motion equation  $22.2798\ddot{x}(t) + 18.4829\dot{x}(t) + 1571.7874x(t) + 1572.5618z(t) = -22.2798u(t)$ , which in nature is a linear system. This reflects that our proposed framework is capable of automatically discovering a linear equation if the system comes without evident nonlinearity or hysteresis. Figures 14 and 15 show that the model closely matches the training and testing responses in terms of displacement,

velocity, and acceleration. Table 6 provides quantitative results. The small NRMSEs confirm that the framework achieves accurate and robust identification when the hysteresis is mild and rate-dominated.

For the *with NSD* case, the hysteresis loops become much wider and exhibit obvious pinching and asymmetry (Figure 13 (b)). Accordingly, the learned  $\dot{z}(t)$  includes higher-order and mixed-magnitude terms of  $x(t)$ ,  $\dot{x}(t)$ , and  $z(t)$ . The predicted hysteretic link equation is  $\dot{z}(t) = 4.8586\dot{x}(t) + 1.6412x^2|\dot{x}(t)| + 1.8160\dot{x}(t)|\dot{x}(t)|z(t) - 1.8174\dot{x}(t)|z(t)| + 1.7648z(t)|z(t)|$  with the dynamics motion equation  $22.2798\ddot{x}(t) + 44.7281\dot{x}(t) + 2099.6526x(t) + 2108.1516z(t) = -22.2798u(t)$ . As shown in Figures 16 and 17, the training responses are well captured, but testing displacement exhibits larger deviations. Table 6 confirms this: the displacement error rises to 14.11% in the testing set, while velocity and acceleration remain within 6%. This indicates that the NSD introduces stronger nonlinear hysteresis, which requires a richer  $\dot{z}$  structure and leads to a larger generalization gap. In other words, the model still succeeds in capturing the main nonlinear patterns, but the predictive accuracy is more sensitive to unseen excitations.

From all these results, it can be concluded that the proposed framework is capable of both equation discovery and dynamic prediction in real experimental data. For the relatively simple *without NSD* case, it achieves concise and highly accurate identification, while for the more challenging *with NSD* case, it still provides interpretable governing equations and meaningful forward predictions, albeit with a higher generalization error. In future work, these limitations may be further addressed by extending the framework toward more complex hysteretic systems and improving its generalization to a wider range of nonlinear dynamical problems.

Table 6: NRMSE results of yielding structure data.

Scenarios	Responses	Training	Testing	Training	Testing
		NRMSE (Ours)	NRMSE (Ours)	NRMSE (Sparse [28])	NRMSE (Sparse [28])
Without NSD	Displacement $x$	3.23%	2.99%	10.73%	2.90%
	Velocity $\dot{x}$	2.57%	2.89%	4.47%	2.92%
	Acceleration $\ddot{x}$	1.45%	2.14%	4.42%	2.70%
With NSD	Displacement $x$	4.12%	14.11%	6.57%	13.85%
	Velocity $\dot{x}$	4.49%	5.60%	4.56%	5.62%
	Acceleration $\ddot{x}$	5.96%	4.86%	5.71%	6.26%

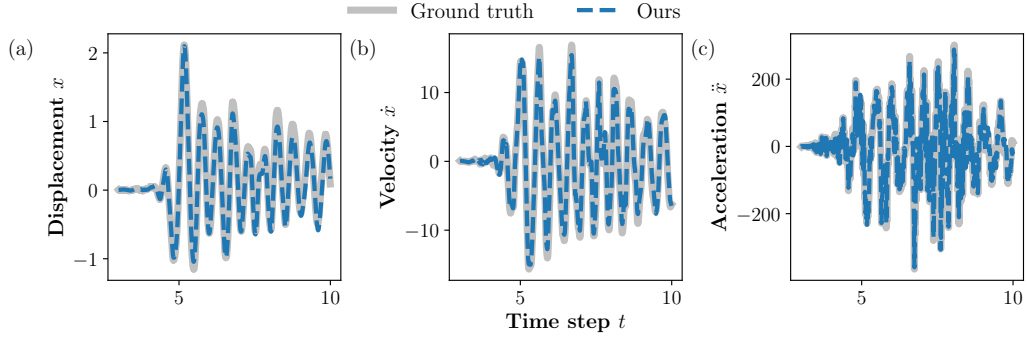


Figure 14: Training results of yielding structure data without NSD. (a) Displacement results. (b) Velocity results. (c) Acceleration results.

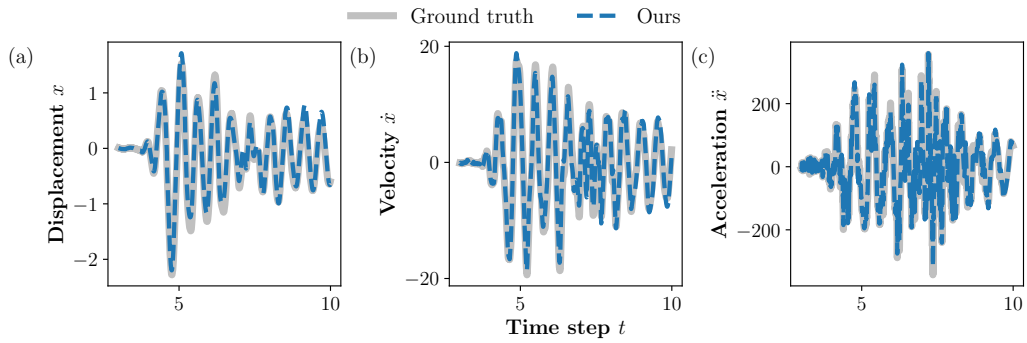


Figure 15: Testing results of yielding structure data without NSD. (a) Displacement results. (b) Velocity results. (c) Acceleration results.

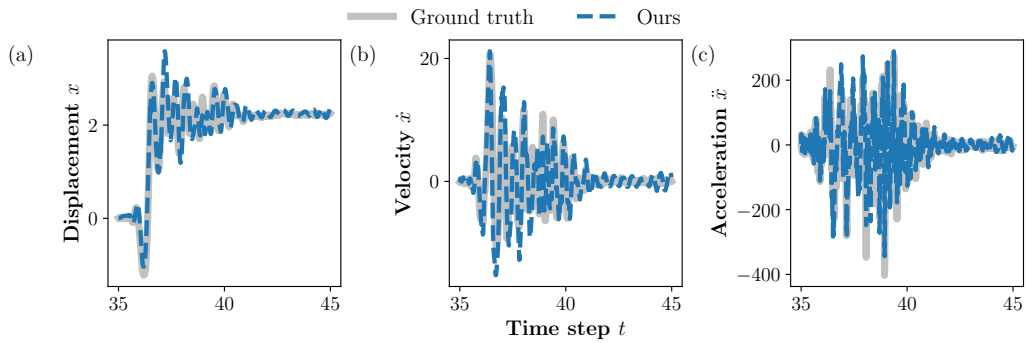


Figure 16: Training results of yielding structure data with NSD. (a) Displacement results. (b) Velocity results. (c) Acceleration results.

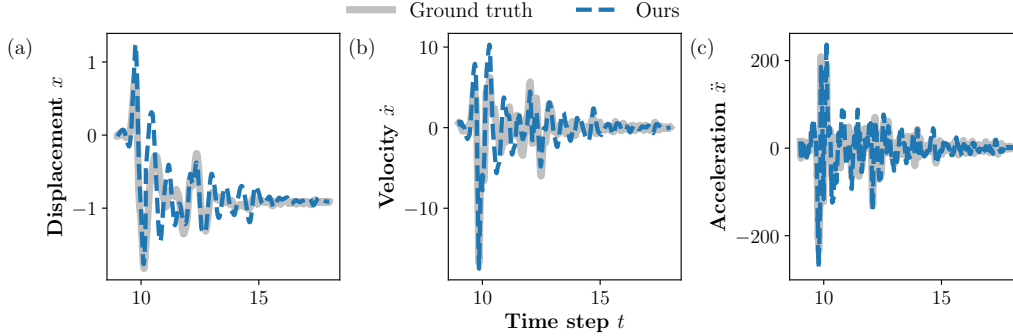


Figure 17: Testing results of yielding structure data with NSD. (a) Displacement results. (b) Velocity results. (c) Acceleration results.

#### 4.4. Extension to MDOF systems

The proposed framework for equation discovery and dynamic prediction is not restricted to SDOF hysteretic systems. For an MDOF system [51, 52], we promote the vector states to the matrix and represent the coupled dynamics ( $t$  is omitted for brevity in this section) with  $r$ -DOF and  $q$  hysteretic variable(s). Therefore, the equations can be written as:

$$\begin{cases} \mathbf{M}\ddot{\mathbf{x}} + \mathbf{C}\dot{\mathbf{x}} + \mathbf{K}\mathbf{x} + \mathbf{H}\mathbf{z} = \mathbf{B}\mathbf{u}, \\ \dot{\mathbf{z}} = \mathbf{g}_\phi(\dot{\mathbf{x}}, \mathbf{z}), \end{cases} \quad (17)$$

where  $\mathbf{x} \in \mathbb{R}^r$  denotes the displacement vector (with  $r$ -DOF), and  $\mathbf{z} \in \mathbb{R}^q$  collects the hysteretic variables associated with localized hysteretic elements (e.g., inter-story links, yielding dampers, or absorber components). The matrices  $\mathbf{M}, \mathbf{C}, \mathbf{K} \in \mathbb{R}^{r \times r}$  are the mass, damping, and stiffness matrices, respectively. The coupling matrix  $\mathbf{H} \in \mathbb{R}^{r \times q}$  maps the hysteretic variables to generalized restoring forces, while  $\mathbf{B} \in \mathbb{R}^{r \times p}$  distributes the external input  $\mathbf{u} \in \mathbb{R}^p$  to the structural DOFs. The (possibly nonlinear) function  $\mathbf{g}_\phi$  governs the hysteretic variable evolution and can encode rate dependence and memory effects.

To illustrate the above formulation, we consider a simple yet representative case with  $r = 2, q = 1$  and  $p = 1$ , corresponding to a 2-DOF model equipped with a single hysteretic energy-dissipating link. Let:

$$\mathbf{x} = \begin{bmatrix} x_1 \\ x_2 \end{bmatrix}, \quad z \in \mathbb{R}, \quad (18)$$

where  $x_1$  and  $x_2$  are the displacements of the 2-DOFs, and  $z$  represents the hysteretic variable. The coupled dynamics in Eq.(17) can be reduce to:

$$\begin{cases} \mathbf{M}\ddot{\mathbf{x}} + \mathbf{C}\dot{\mathbf{x}} + \mathbf{K}\mathbf{x} + \mathbf{H}z = \mathbf{B}u, \\ \dot{z} = g_\phi(\dot{x}_1, \dot{x}_2, z). \end{cases} \quad (19)$$

As a concrete numerical example, we choose a harmonic excitation  $u(t) = 1000 \sin(2\pi \times 1.5t)$  and  $\mathbf{B} = [1, 1]^T$ , specify:

$$\mathbf{M} = \begin{bmatrix} m_1 & 0 \\ 0 & m_2 \end{bmatrix} = \begin{bmatrix} 100 & 0 \\ 0 & 80 \end{bmatrix}, \quad \mathbf{C} = \begin{bmatrix} c_{11} & c_{12} \\ c_{21} & c_{22} \end{bmatrix} = \begin{bmatrix} 30 & -5 \\ -5 & 20 \end{bmatrix}, \quad (20)$$

$$\mathbf{K} = \begin{bmatrix} k_{11} & k_{12} \\ k_{21} & k_{22} \end{bmatrix} = \begin{bmatrix} 3500 & -1500 \\ -1500 & 1500 \end{bmatrix}, \quad \mathbf{H} = \begin{bmatrix} h_1 \\ h_2 \end{bmatrix} = \begin{bmatrix} 1 \\ -1 \end{bmatrix}. \quad (21)$$

With this choice, the hysteretic link exerts equal and opposite restoring forces on the 2-DOFs. For the hysteretic variable evolution, we adopt a simple rate-dependent form driven by the inter-story relative velocity  $\dot{x}_2 - \dot{x}_1$ :

$$\dot{z} = a(\dot{x}_2 - \dot{x}_1) - b|\dot{x}_2 - \dot{x}_1| z, \quad a = 50, \quad b = 2. \quad (22)$$

For completeness, Eq.(19) can be written component-wise as:

$$\begin{cases} 100 \ddot{x}_1 + 30 \dot{x}_1 - 5 \dot{x}_2 + 3500 x_1 - 1500 x_2 + z = u, \\ 80 \ddot{x}_2 - 5 \dot{x}_1 + 20 \dot{x}_2 - 1500 x_1 + 1500 x_2 - z = u, \\ \dot{z} = 50(\dot{x}_2 - \dot{x}_1) - 2|\dot{x}_2 - \dot{x}_1| z, \end{cases} \quad (23)$$

which represent the dynamic motion equation  $f_{\theta_1}, f_{\theta_2}$  and the hysteretic link equation  $g_\phi$ , respectively.

The above derivations illustrate that the adopted state-space formulations extend naturally to MDOF settings by treating both structural states and hysteretic variables in a coupled form. Therefore, the formulation remains structurally identical to the SDOF case, with the equation discovery task now applied to Eq.(23). In what follows, we present the *Hysteresis Discovery* case in Figure 1, where the measurements are noise-free and  $\mathbf{x}$ ,  $\dot{\mathbf{x}}$ , and  $\ddot{\mathbf{x}}$  are all known, and the other settings are similar. Combining the procedure in the proposed framework, the unknowns include the entries of  $\mathbf{M}$ ,  $\mathbf{C}$ ,  $\mathbf{K}$ , and  $\mathbf{H}$ , as well as the entire functional form of the hysteretic-variable evolution

in Eq.(22). Using the strategy of reformulation introduced in Section 3, the MDOF formulation can be written explicitly in a first-order state-space form:

$$\frac{d}{dt} \begin{bmatrix} x_1 \\ x_2 \\ \dot{x}_1 \\ \dot{x}_2 \end{bmatrix} = \begin{bmatrix} \dot{x}_1 \\ \dot{x}_2 \\ f_{\theta_1} \\ f_{\theta_2} \end{bmatrix}, \quad (24)$$

with  $z$  being trainable.

The discovered governing equations and NRMSE results can be seen in Table 7 and 8. Figure 18 shows the training and testing results of the discovered MDOF system for both displacement and velocity responses. These results indicate that the proposed framework remains effective when extended from SDOF to MDOF systems, yielding reasonably accurate equation discovery and dynamic predictions.

We acknowledge that, as in many MDOF settings, the problem becomes increasingly complex as the number of DOF grows. As  $r$  and  $q$  increase, both computational cost and identifiability challenges can become more pronounced, especially when hysteresis is present in multiple or adjacent DOFs due to structural coupling. Nevertheless, based on above observations, the proposed framework remains directly applicable and can handle this increased complexity.

Table 7: Discovered governing equations of the MDOF hysteretic system.

Type	Equation
True $f_{\theta_1}$	$100.0000 \ddot{x}_1 + 30.0000 \dot{x}_1 - 5.0000 \dot{x}_2 + 3500.0000 x_1 - 1500 x_2 + 1.0000 z = u$
Discovered $f_{\theta_1}$	$94.9694 \ddot{x}_1 + 31.5296 \dot{x}_1 - 4.7204 \dot{x}_2 + 3325.0000 x_1 - 1574.9634 x_2 + 0.9799 z = u$
True $f_{\theta_2}$	$80.0000 \ddot{x}_2 - 5.0000 \dot{x}_1 + 20.0000 \dot{x}_2 - 1500.0000 x_1 + 1500 x_2 - 1.0000 z = u$
Discovered $f_{\theta_2}$	$83.9695 \ddot{x}_2 - 5.2208 \dot{x}_1 + 19.0294 \dot{x}_2 - 1424.9634 x_1 + 1575.0122 x_2 - 1.0200 z = u$
True $g_\phi$	$\dot{z} = 50.0000(\dot{x}_2 - \dot{x}_1) - 2.0000  \dot{x}_2 - \dot{x}_1  z$
Discovered $g_\phi$	$\dot{z} = 46.1250(\dot{x}_2 - \dot{x}_1) - 2.3642  \dot{x}_2 - \dot{x}_1  z$

Table 8: NRMSE results of MDOF hysteretic system.

Responses	Training NRMSE	Testing NRMSE
Displacement $x_1$	2.55%	5.99%
Displacement $x_2$	1.35%	3.73%
Velocity $\dot{x}_1$	3.44%	4.97%
Velocity $\dot{x}_2$	2.95%	2.09%

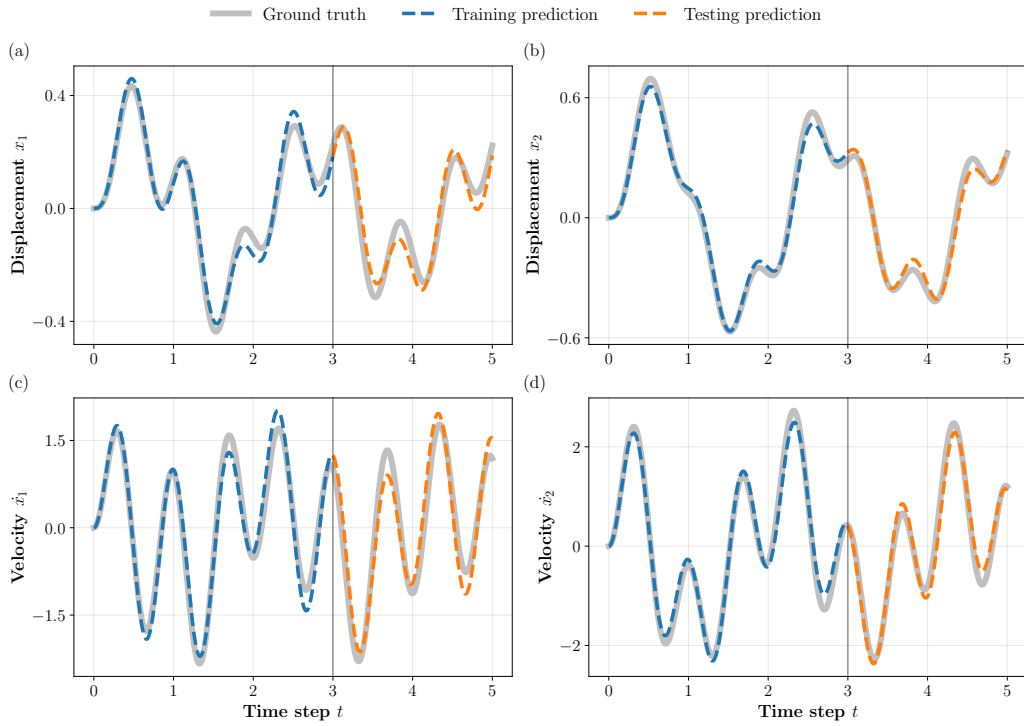


Figure 18: Training and testing results of the MDOF system. The time interval 0–3s is used for training, and 3–5s is used for testing. (a)&(b) Displacement results. (c)&(d) Velocity results.

## 5. Conclusion

This research presented a unified framework for equation discovery and dynamic prediction of hysteretic systems, with a proposed solver-based hysteretic variable learning scheme that addresses one of the key challenges in hysteresis modeling – the difficulty of inferring hysteretic variables. We summarize existing work on equation discovery for hysteretic systems and categorize them according to the level of assumed knowledge available. The proposed unified framework in our work is capable of addressing two major challenges of hysteretic systems across various scenarios: the learning of unobservable hysteretic variables and the discovery of governing equations with complex nonlinear expressions. The effectiveness of the framework is validated through four representative case studies. On the Bouc-Wen benchmark, it accurately recovers the governing equations even in the presence of noise, confirming its robustness and reliability. For a more complex nonlinear structure with cubic stiffness and fractional hysteretic exponents, the framework successfully achieves superior accuracy and interpretability compared with library-based methods such as SINDy and the variational methods. In the real shake-table experiment of a yielding structure, the framework reveals concise rate-dominated dynamics without NSD and more complex nonlinear hysteresis behavior with NSD, achieving stable predictions. The extension to MDOF systems shows that the proposed framework is readily extensible to higher-dimensional settings, highlighting its scalability and broader applicability.

This research not only provides insights into equation discovery and dynamic prediction of hysteretic systems but also demonstrates the potential of the proposed framework for broader applications in nonlinear dynamical systems, including those with or without hysteretic variables. Its flexibility and interpretability make it applicable to various domains such as structural dynamics, material modeling, and control system identification, where nonlinear and memory-dependent behaviors are common. In addition, although the framework has extended the validation to fractional and MDOF settings, further investigation of additional hysteresis families, such as strongly asymmetric, severely pinched, S-shaped, or flag-shaped loops, remains important in the future. Future work will focus on enhancing the efficiency and scalability of the framework, improving its ability to handle more complex systems, and exploring probabilistic or hybrid modeling strategies to further extend its applicability to real-world engineering and scientific problems.

## Acknowledgments

The authors would like to express their sincere gratitude to Prof. Satish Nagarajaiah at Rice University for generously sharing the experimental SDOF yielding structure data that made this research possible. The authors wish to express their gratitude for the financial support received from Guangdong Provincial Fund - Special Innovation Project (2024KTSCX038); Research Grants Council of Hong Kong through the Research Impact Fund (R5006-23); Guangdong Provincial Key Lab of Integrated Communication, Sensing and Computation for Ubiquitous Internet of Things (No. 2023B1212010007); Natural Science Foundation of Guangdong Province, China (General Fund; Grant No. 2026A1515011629).

## Appendix A. Network architecture and training details

In this work implementation,  $\mathcal{N}_\theta(\cdot)$  in *Full Equation Discovery* is parameterized as a multilayer perceptron with two hidden layers, each of width 128, and hyperbolic tangent activation functions. The network parameters are optimized jointly within the solver-based training procedure using the Adam algorithm, with a learning rate of  $3 \times 10^{-4}$ , first- and second-moment decay rates of 0.9 and 0.98, respectively, and an  $\ell_2$  regularization coefficient of  $10^{-4}$ . To improve optimization stability, gradient norm clipping with a threshold of 1.0 is applied. Training is terminated either upon convergence of the loss or when a prescribed maximum number of iterations (e.g., 10,000) is reached.

## Appendix B. Computational complexity and scalability

We briefly discuss computational complexity and scalability as the system dimension increases. Let  $r$  denote the number of degrees of freedom (DOFs),  $q$  the number of hysteretic variables, and  $N$  the total number of sampled time points.

### *Appendix B.1. Step 1: Solver-based hysteretic variable learning.*

At this step, the trainable hysteretic variable is learned by embedding the governing dynamics into a differentiable ODE solver and jointly optimizing the model parameters and the trainable hysteretic variables through trajectory matching. Since the trainable hysteretic variable is parameterized

outside the solver (shown in Figure 2), the embedded solver advances only the displacement and velocity states, so the solver state has dimension  $2r$ . For each optimization iteration, the solver is unrolled over  $N$  time samples, and the trainable hysteretic variable is injected into the motion equation at the corresponding sampled times. If the solver uses  $n_s$  stage evaluations per time step, with  $n_s = 4$  for RK4, the per-iteration solver cost is  $\mathcal{O}(Nn_s 2r)$ , while updating the trainable hysteretic variables over all time samples introduces an additional cost of  $\mathcal{O}(Nq)$  per iteration. Hence, the per-iteration computational cost is  $\mathcal{O}(Nn_s 2r + Nq)$ . Since  $n_s$  is typically small and fixed in practice, this can be simplified to:

$$\mathcal{O}(N(2r + q)). \quad (\text{B.1})$$

*Appendix B.2. Step 2: Equation discovery.*

At this step, SR is applied to the learned trajectories to recover explicit governing equations. The computational cost is dominated by the symbolic search process. Let  $P$  denote the population size and  $G$  the number of generations. For each candidate symbolic expression, the main cost comes from evaluating the expression over the available data samples. If  $C$  denotes the per-sample cost of evaluating one candidate symbolic expression, then the computational cost of Step 2 is:

$$\mathcal{O}(NPGC). \quad (\text{B.2})$$

Relative to conventional gradient-based parameter estimation for a prescribed hysteretic model, the proposed Step 1 shares a similar computational backbone, as both require repeated forward ODE integration and gradient-based optimization over trajectory data. However, the present framework is generally more computationally demanding in practice because the hysteretic relation is not fixed a priori and must instead be learned in a more flexible function space, rather than calibrated through a small set of prescribed physical parameters. In addition, the proposed framework introduces an offline Step 2 after training. These additional computational costs represent a trade-off for reduced structural assumptions and the ability to recover an interpretable symbolic governing equation.

*Appendix B.3. Impact of multiple hysteretic variables.*

When hysteresis is present at multiple or adjacent DOFs, different hysteretic variables may contribute to overlapping restoring-force components

because of structural coupling. As a result, similar observable responses can be explained by different combinations of hysteretic variables, which makes the different hysteretic contributions harder to identify and renders the joint optimization more ill-conditioned. From both computational and identifiability perspectives, scalability therefore relies not only on computational resources, but also on sufficiently informative excitations, multiple training trajectories, adequate sensing, and physically motivated regularization (e.g., sparsity or locality in cross-DOF coupling) to stabilize learning and improve the separability of hysteretic contributions.

### **Appendix C. Additional experiments on the Bouc-Wen hysteretic system benchmark**

To further validate the effectiveness and practical applicability of the proposed framework, we conduct some additional benchmark experiments beyond the baseline setting.

#### *Appendix C.1. Cross-excitation validation*

To assess whether the discovered equations are biased to a specific excitation history, we swapped the training and testing roles of the two excitation signals used in the baseline in the medium-noise setting (SNR = 20 dB). Specifically, the multisine signal is used for training and the sinesweep signal for testing, i.e., the reverse of the setting shown in Figure 3. For a fair comparison, all remaining training settings (data length, sampling rate, optimization hyperparameters, etc.) are kept identical to the baseline.

For quantitative evaluation, Table C.9 reports the NRMSE results, together with discovered equations  $1.7803\ddot{x} + 8.0472\dot{x} + 47360.7258x + 0.8736z = u$  and  $\dot{z} = 57072.5992\dot{x} - 748.504|\dot{x}|z + 748.504\dot{x}|z|$ . Figures C.19 and C.20 visualize the predicted responses against the ground truth in the swapped excitation setting. In this cross-excitation validation example, the proposed framework maintains competitive accuracy for both seen and unseen excitation types, suggesting that the discovered equations are not related to a specific input history and retain predictive capability across the two benchmark excitation types.

#### *Appendix C.2. Extrapolation test on unseen amplified excitation*

To evaluate performance beyond the training operating range, we keep the same medium-noise baseline setting and test the discovered equations

Table C.9: NRMSE results for the cross-excitation validation and extrapolation tests on the benchmark system.

Category	Responses	Training NRMSE	Testing 1 NRMSE	Testing 2 NRMSE
Baseline	Displacement $x$	2.41%	1.64%	3.30%
	Velocity $\dot{x}$	3.08%	2.15%	3.37%
Cross-excitation validation	Displacement $x$	2.71%	3.03%	3.20%
	Velocity $\dot{x}$	3.11%	3.13%	2.87%
Extrapolation test	Displacement $x$	–	1.93%	3.24%
	Velocity $\dot{x}$	–	2.63%	3.77%

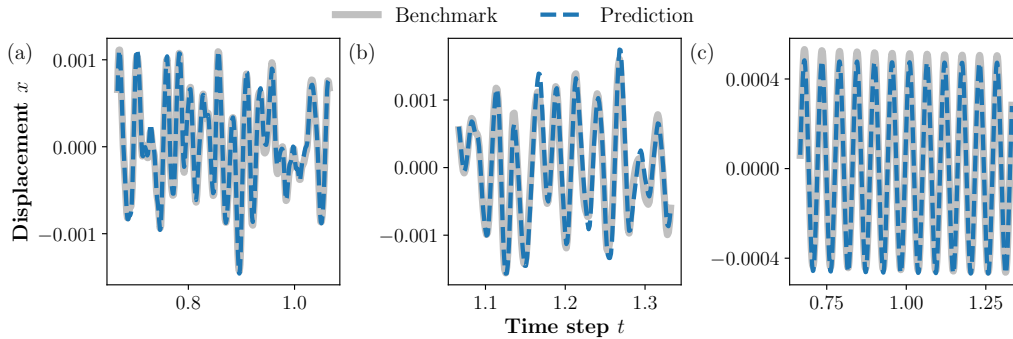


Figure C.19: Displacement results on the benchmark system - cross-excitation validation. In contrast to Figure 5, the multisine signal is used as the training input, while the sinesweep signal is used as the testing input. (a) Training results. (b) Testing 1 (same excitation) results. (c) Testing 2 (unseen excitation) results.

under an amplitude-scaled excitation without retraining. In contrast to the nominal testing condition, we construct an amplitude-extrapolated test input by scaling the multisine excitation by a factor of 1.5, while keeping all other settings unchanged. Without retraining or re-identification, we evaluate the governing equations obtained under the baseline setting.

The quantitative NRMSE results are summarized in Table C.9, and the corresponding displacement and velocity comparisons are visualized in Figures. C.21 and C.22. From this example, the proposed framework remains stable under the increased excitation amplitude and achieves accuracy comparable to that under the nominal testing condition, indicating reasonable extrapolation capability within the considered amplitude range.

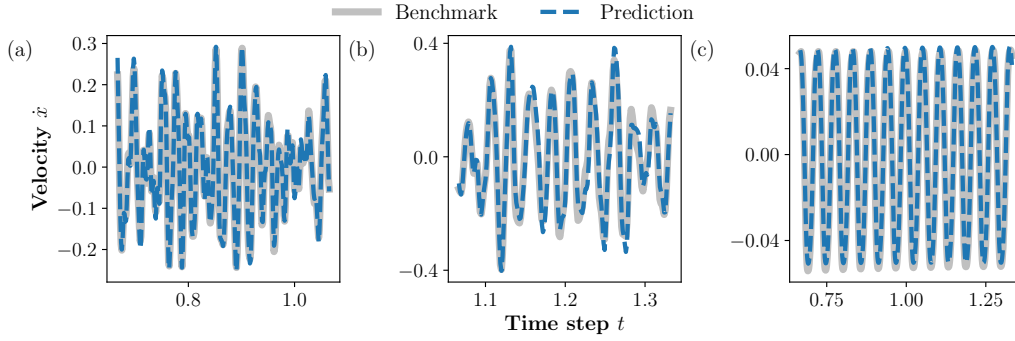


Figure C.20: Velocity results on the benchmark system - cross-excitation validation. In contrast to Figure 6, the multisine signal is used as the training input, while the sinesweep signal is used as the testing input. (a) Training results. (b) Testing 1 (same excitation) results. (c) Testing 2 (unseen excitation) results.

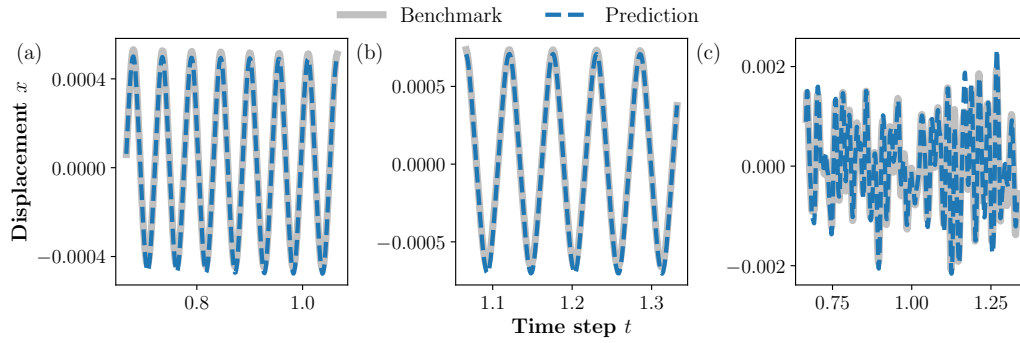


Figure C.21: Displacement results on the benchmark system - extrapolation test. In contrast to Figure 5, the multisine excitation used for testing is amplitude-scaled by a factor of 1.5. (a) Training results. (b) Testing 1 (same excitation) results. (c) Testing 2 (unseen excitation) results.

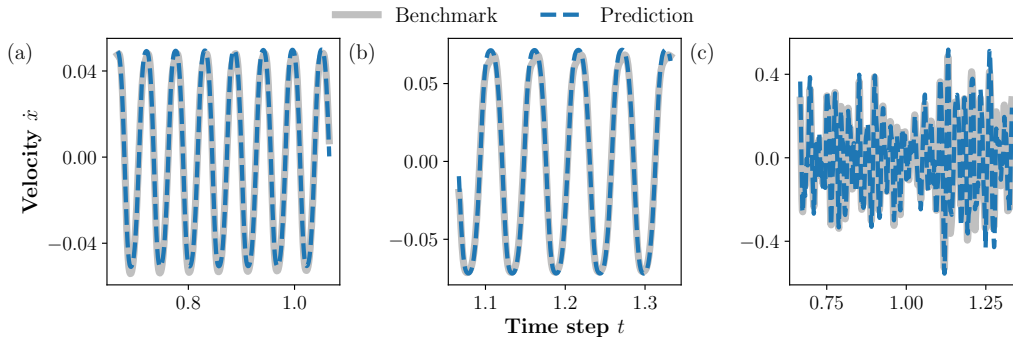


Figure C.22: Velocity results on the benchmark system - extrapolation test. In contrast to Figure 6, the multisine excitation used for testing is amplitude-scaled by a factor of 1.5. (a) Training results. (b) Testing 1 (same excitation) results. (c) Testing 2 (unseen excitation) results.

### Appendix C.3. Sensitivity analyses

To evaluate robustness to modest parameter mismatch, we keep the training procedure unchanged and perturb the true system parameters only at test time by applying a  $\pm 5\%$  drift to  $c$  or  $k$  while holding the other parameter at its nominal value.

The quantitative results are summarized in Table C.10 in terms of NRMSE for both displacement and velocity responses. The performance degradation caused by perturbing  $k$  is noticeably larger than that induced by perturbing  $c$ , indicating that the system responses are more sensitive to stiffness variations in this benchmark. A plausible reason is that stiffness directly determines the restoring-force scale and the oscillation characteristics of the system, whereas damping primarily influences the rate of energy dissipation. Even under these small parameter drifts, the framework maintains reasonably low NRMSE values across both testing cases, indicating robust predictive performance in the presence of mild parameter uncertainty.

Table C.10: NRMSE results of the sensitivity analyses under  $\pm 5\%$  test-time parameter drift on the benchmark system.

Setting	Responses	Testing 1 NRMSE	Testing 2 NRMSE
Baseline (nominal $c, k$ )	Displacement $x$	1.64%	3.30%
	Velocity $\dot{x}$	2.15%	3.37%
$c \uparrow 5\%$ , $k$ nominal	Displacement $x$	2.08%	3.52%
	Velocity $\dot{x}$	2.31%	3.61%
$c \downarrow 5\%$ , $k$ nominal	Displacement $x$	2.38%	3.60%
	Velocity $\dot{x}$	2.46%	3.97%
$c$ nominal, $k \uparrow 5\%$	Displacement $x$	3.28%	4.81%
	Velocity $\dot{x}$	3.97%	4.96%
$c$ nominal, $k \downarrow 5\%$	Displacement $x$	3.67%	4.64%
	Velocity $\dot{x}$	3.51%	4.72%

#### Appendix C.4. Noisy wideband random excitation training

To assess whether the proposed framework is suitable for noisy and new excitation, a band-limited wideband random excitation is synthesized in the frequency domain and transformed back to the time domain, after which measurement noise is added to emulate a noisy input signal. The same medium-noise setting is adopted for both the system responses and the excitation measurement.

Table C.11 reports the NRMSE results. In this experiment, the model is trained with an excitation signal different from that in the baseline, while the testing excitation is kept unchanged for a fair comparison. Figures C.23 and C.24 visualize the predicted displacement and velocity responses. The results show that the proposed framework maintains good predictive accuracy under the new and noisy excitation condition.

#### Appendix C.5. Without hysteresis

To further assess practical applicability, we test whether the framework reduces to an appropriate non-hysteretic model when hysteresis is absent. We construct a non-hysteretic benchmark by setting  $\beta = 0$  and  $\gamma = 0$  in Eq.(15), so that the hysteretic link equation reduces to  $\dot{z}(t) = A\dot{x}(t)$ . Neglecting the integration constant, we obtain  $z(t) = Ax(t)$ . Therefore, the true Eq.(15) is

Table C.11: NRMSE results for the robustness extension experiments on the benchmark system.

Category	Responses	Training NRMSE	Testing 1 NRMSE	Testing 2 NRMSE
Baseline	Displacement $x$	2.41%	1.64%	3.30%
	Velocity $\dot{x}$	3.08%	2.15%	3.37%
Noisy wideband random excitation training	Displacement $x$	2.18%	2.94%	3.11%
	Velocity $\dot{x}$	2.17%	3.00%	2.23%
Without hysteresis	Displacement $x$	0.88%	0.87%	0.82%
	Velocity $\dot{x}$	0.61%	1.04%	0.77%

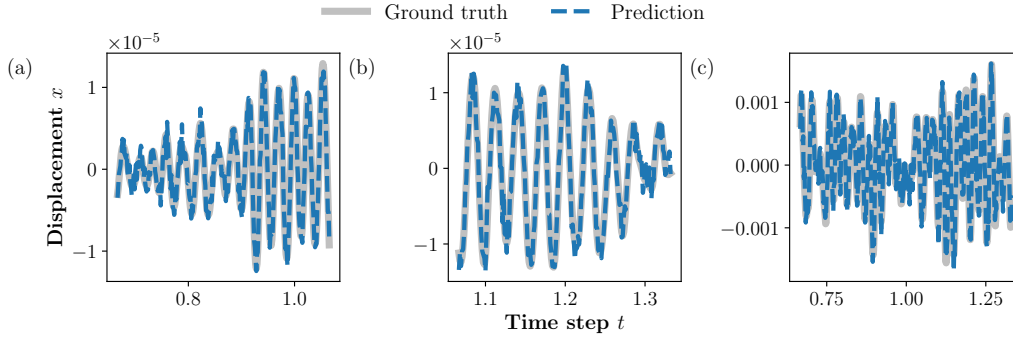


Figure C.23: Displacement results on the benchmark system - noisy wideband random excitation training. (a) Training results. (b) Testing 1 (same excitation) results. (c) Testing 2 (unseen excitation) results.

$2\ddot{x}(t) + 10\dot{x}(t) + 100000x(t) = u(t)$ , degenerate to a non-hysteretic case. All other training and evaluation settings are kept identical to baseline.

In this without hysteresis experiment, the discovered dynamic motion equation is  $1.9998\ddot{x}(t) + 10.0049\dot{x}(t) + 49999.4985x(t) + 1.0089z(t) = u(t)$ , and the discovered hysteretic link equation is  $\dot{z}(t) = 49999.5616\dot{x}(t)$ . Substituting the hysteretic link relation into the motion equation yields the degenerate non-hysteretic form  $1.9998\ddot{x}(t) + 10.0049\dot{x}(t) + 100444.0562x(t) = u(t)$ , which is consistent with the expected non-hysteretic reduction. Figure C.25 shows the hysteresis loops. In panel (c),  $F = kx + \alpha z = (k + A)x$ , and panels (b) and (c) clearly exhibit an approximately linear relationship in the degenerate regime, consistent with the above analysis. The NRMSE results in Table C.11 further confirm that the proposed framework remains accurate when the

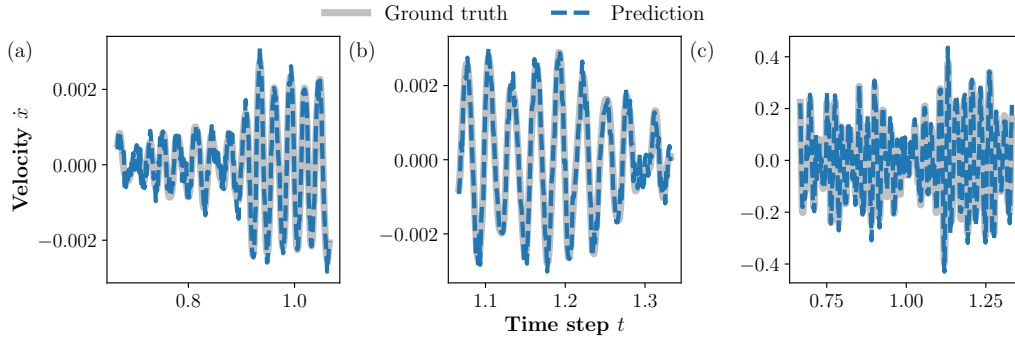


Figure C.24: Velocity results on the benchmark system - noisy wideband random excitation training. (a) Training results. (b) Testing 1 (same excitation) results. (c) Testing 2 (unseen excitation) results.

dynamics reduce to the simpler non-hysteretic case. This is also supported by the response comparisons in Figures C.26 and C.27. These results further support the unified nature of the proposed framework, which can recover both hysteretic and degenerate non-hysteretic dynamics without requiring a prescribed model structure.

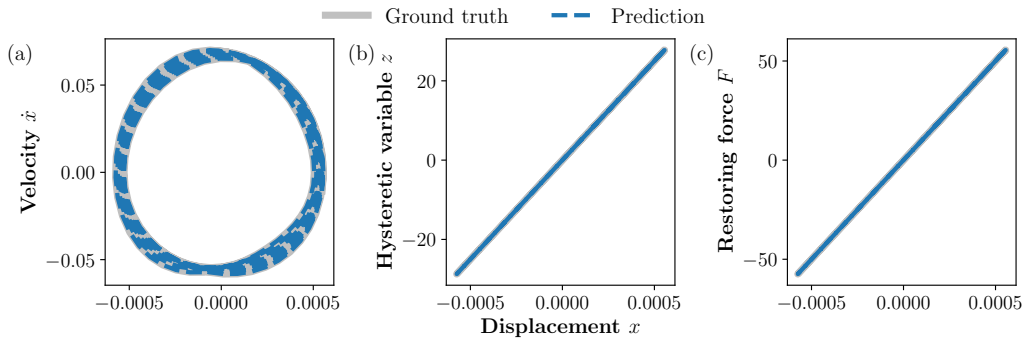


Figure C.25: Hysteresis loops on the benchmark system - without hysteresis. (a)  $x - \dot{x}$  hysteresis loop. (b)  $x - z$  hysteresis loop. (c)  $x - F(F = (k + A)x)$  hysteresis loop.

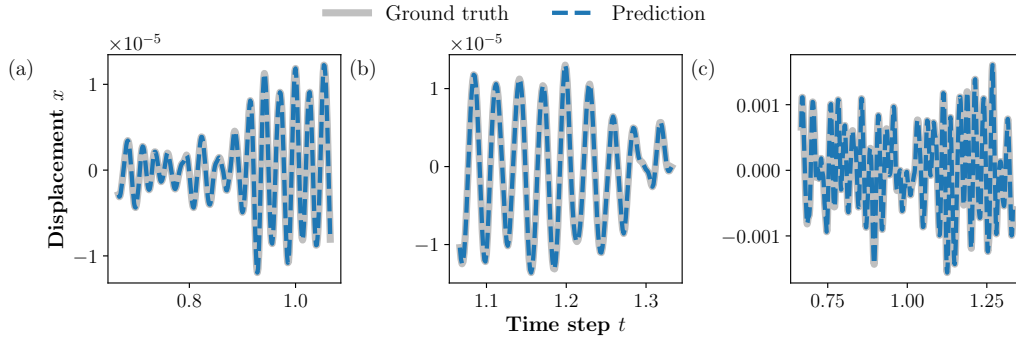


Figure C.26: Displacement results on the benchmark system - without hysteresis. (a) Training results. (b) Testing 1 (same excitation) results. (c) Testing 2 (unseen excitation) results.

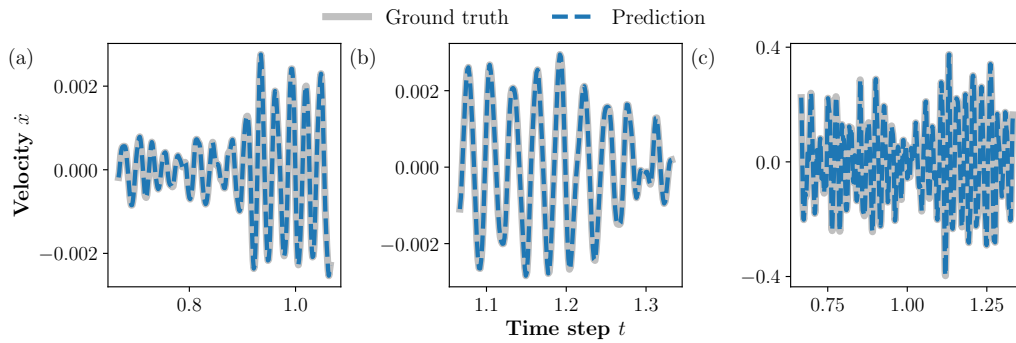


Figure C.27: Velocity results on the benchmark system - without hysteresis. (a) Training results. (b) Testing 1 (same excitation) results. (c) Testing 2 (unseen excitation) results.

## References

- [1] D. C. Jiles, D. L. Atherton, Theory of ferromagnetic hysteresis, *Journal of magnetism and magnetic materials* 61 (1-2) (1986) 48–60.
- [2] M. Al Janaideh, C.-Y. Su, S. Rakehja, Modeling hysteresis of smart actuators, in: *2008 5th International Symposium on Mechatronics and Its Applications*, IEEE, 2008, pp. 1–4.
- [3] G. Bertotti, *Hysteresis in magnetism: for physicists, materials scientists, and engineers*, Academic press, 1998.
- [4] E. Ko, I. Kimura, P. Clark, I. Aiken, K. Kasai, Design procedures for buildings incorporating hysteretic damping devices, in: *Proceedings of the 68th Annual Convention SEAOC*, Santa Barbara, CA, USA, Vol. 30, 1999.
- [5] A. Dominguez, R. Sedaghati, I. Stiharu, Modelling the hysteresis phenomenon of magnetorheological dampers, *Smart Materials and Structures* 13 (6) (2004) 1351.
- [6] J. Ortín, L. Delaey, Hysteresis in shape-memory alloys, *International Journal of Non-Linear Mechanics* 37 (8) (2002) 1275–1281.
- [7] Y.-K. Wen, Method for random vibration of hysteretic systems, *Journal of the engineering mechanics division* 102 (2) (1976) 249–263.
- [8] C. Visone, Hysteresis modelling and compensation for smart sensors and actuators, in: *Journal of Physics: Conference Series*, Vol. 138, IOP Publishing, 2008, p. 012028.
- [9] E. N. Chatzi, A. W. Smyth, S. F. Masri, Experimental application of on-line parametric identification for nonlinear hysteretic systems with model uncertainty, *Structural Safety* 32 (5) (2010) 326–337.
- [10] A. Chandra, B. Daniels, M. Curti, K. Tiels, E. A. Lomonova, D. M. Tartakovsky, Discovery of sparse hysteresis models for piezoelectric materials, *Applied Physics Letters* 122 (21) (2023).

- [11] Y. Liu, K. P. Kelley, R. K. Vasudevan, H. Funakubo, M. A. Ziatdinov, S. V. Kalinin, Experimental discovery of structure–property relationships in ferroelectric materials via active learning, *Nature Machine Intelligence* 4 (4) (2022) 341–350.
- [12] K. Vlachas, K. Agathos, K. E. Tatsis, A. R. Brink, E. Chatzi, Two-story frame with bouc-wen hysteretic links as a multi-degree of freedom nonlinear response simulator, in: *5th Workshop on Nonlinear System Identification Benchmarks*, ETH Zurich, 2021.
- [13] R. Capuano, A. Fraddosio, M. D. Piccioni, Phenomenological rate-independent uniaxial hysteretic models: A mini-review, *Frontiers in Built Environment* 8 (2022) 1048533.
- [14] R. Capuano, N. Vaiana, B. Carboni, A generalized bouc–wen model for simulating the quasi-static and dynamic shear responses of helical wire rope isolators, *Nonlinear Dynamics* 112 (21) (2024) 18701–18715.
- [15] N. Vaiana, L. Rosati, Analytical and differential reformulations of the vaiana–rosati model for complex rate-independent mechanical hysteresis phenomena, *Mechanical Systems and Signal Processing* 199 (2023) 110448.
- [16] N. Vaiana, L. Rosati, Classification and unified phenomenological modeling of complex uniaxial rate-independent hysteretic responses, *Mechanical Systems and Signal Processing* 182 (2023) 109539.
- [17] S. H. Rudy, S. L. Brunton, J. L. Proctor, J. N. Kutz, Data-driven discovery of partial differential equations, *Science advances* 3 (4) (2017) e1602614.
- [18] B. Chen, C. Zhang, J. Zhang, Y. Wang, Adaptive physics-informed system modeling with control for nonlinear structural system estimation, *Computer Methods in Applied Mechanics and Engineering* 447 (2025) 118330.
- [19] M. Haywood-Alexander, W. Liu, K. Bacsá, Z. Lai, E. Chatzi, Discussing the spectrum of physics-enhanced machine learning: a survey on structural mechanics applications, *Data-Centric Engineering* 5 (2024) e30.

- [20] L. Yi, S. Yang, Y. Cui, Z. Lai, Transforming physics-informed machine learning to convex optimization, *Engineering Applications of Artificial Intelligence* 161 (2025) 112149.
- [21] S. Yang, C. Song, Z. Lai, W. Wang, KP-PINNs: Kernel packet accelerated physics informed neural networks, in: *Proceedings of the Thirty-Fourth International Joint Conference on Artificial Intelligence, IJCAI-25, 2025*, pp. 7904–7912.
- [22] L. Yan, H. Cai, Q. Wang, L. Chen, C. Li, G. Hu, Deep reinforcement learning-based active flow control for a tall building, *Physics of Fluids* 37 (4) (2025).
- [23] K. Yu, E. Chatzi, G. Kissas, Grammar-based ordinary differential equation discovery, *Mechanical Systems and Signal Processing* 240 (2025) 113395.
- [24] S. L. Brunton, J. L. Proctor, J. N. Kutz, Discovering governing equations from data by sparse identification of nonlinear dynamical systems, *Proceedings of the national academy of sciences* 113 (15) (2016) 3932–3937.
- [25] K. P. Champion, S. L. Brunton, J. N. Kutz, Discovery of nonlinear multiscale systems: Sampling strategies and embeddings, *SIAM Journal on Applied Dynamical Systems* 18 (1) (2019) 312–333.
- [26] Z. Chen, Y. Liu, H. Sun, Physics-informed learning of governing equations from scarce data, *Nature communications* 12 (1) (2021) 6136.
- [27] Q. Liu, J. Cao, Y. Zhang, Z. Zhao, G. Kerschen, X. Jing, Interpretable sparse identification of a bistable nonlinear energy sink, *Mechanical Systems and Signal Processing* 193 (2023) 110254.
- [28] Z. Lai, S. Nagarajaiah, Sparse structural system identification method for nonlinear dynamic systems with hysteresis/inelastic behavior, *Mechanical Systems and Signal Processing* 117 (2019) 813–842.
- [29] D. A. Messenger, D. M. Bortz, Weak sindy: Galerkin-based data-driven model selection, *Multiscale Modeling & Simulation* 19 (3) (2021) 1474–1497.

- [30] K. Kaheman, J. N. Kutz, S. L. Brunton, Sindy-pi: a robust algorithm for parallel implicit sparse identification of nonlinear dynamics, *Proceedings of the Royal Society A* 476 (2242) (2020) 20200279.
- [31] A. Bolourchi, S. F. Masri, O. J. Aldraihem, Studies into computational intelligence and evolutionary approaches for model-free identification of hysteretic systems, *Computer-Aided Civil and Infrastructure Engineering* 30 (5) (2015) 330–346.
- [32] T. Wang, M. Noori, G. Wang, Z. Wu, Symbolic deep learning-based method for modeling complex rate-independent hysteresis, *Computers & Structures* 311 (2025) 107702.
- [33] W. Liu, K. Bacsa, L. C. Tang, E. Chatzi, Structured kolmogorov-arnold neural odes for interpretable learning and symbolic discovery of nonlinear dynamics, *arXiv preprint arXiv:2506.18339* (2025).
- [34] M. Lin, C. Cheng, G. Zhang, B. Zhao, Z. Peng, G. Meng, Identification of bouc-wen hysteretic systems based on a joint optimization approach, *Mechanical Systems and Signal Processing* 180 (2022) 109404.
- [35] K. Worden, J. Hensman, Parameter estimation and model selection for a class of hysteretic systems using bayesian inference, *Mechanical Systems and Signal Processing* 32 (2012) 153–169.
- [36] A. E. Charalampakis, V. K. Koumouisis, Identification of bouc–wen hysteretic systems by a hybrid evolutionary algorithm, *Journal of Sound and Vibration* 314 (3-5) (2008) 571–585.
- [37] J. Qian, X. Sun, J. Xu, L. Cheng, Discovering differential governing equations of hysteresis dynamic systems by data-driven sparse regression method, *Nonlinear Dynamics* 112 (14) (2024) 12137–12157.
- [38] N. M. Newmark, A method of computation for structural dynamics, *Journal of the engineering mechanics division* 85 (3) (1959) 67–94.
- [39] J. C. Butcher, *Numerical methods for ordinary differential equations*, John Wiley & Sons, 2016.
- [40] A. Iserles, *A first course in the numerical analysis of differential equations*, no. 44, Cambridge university press, 2009.

- [41] M. Cranmer, Interpretable machine learning for science with pysr and symbolicregression. jl, arXiv preprint arXiv:2305.01582 (2023).
- [42] M. Quade, M. Abel, K. Shafi, R. K. Niven, B. R. Noack, Prediction of dynamical systems by symbolic regression, *Physical Review E* 94 (1) (2016) 012214.
- [43] J.-P. Noel, M. Schoukens, Hysteretic benchmark with a dynamic non-linearity, in: *Workshop on nonlinear system identification benchmarks*, 2016, pp. 7–14.
- [44] R. Bouc, Forced vibrations of mechanical systems with hysteresis, in: *Proc. of the Fourth Conference on Nonlinear Oscillations*, Prague, 1967, 1967.
- [45] M. Ismail, F. Ikhouane, J. Rodellar, The hysteresis bouc-wen model, a survey, *Archives of computational methods in engineering* 16 (2) (2009) 161–188.
- [46] F. Ikhouane, J. Rodellar, *Systems with hysteresis: analysis, identification and control using the Bouc-Wen model*, John Wiley & Sons, 2007.
- [47] A. A. Sarlis, D. T. R. Pasala, M. Constantinou, A. Reinhorn, S. Nagarajaiah, D. Taylor, Negative stiffness device for seismic protection of structures, *Journal of Structural Engineering* 139 (7) (2013) 1124–1133.
- [48] D. Pasala, A. Sarlis, S. Nagarajaiah, A. Reinhorn, M. Constantinou, D. Taylor, Adaptive negative stiffness: new structural modification approach for seismic protection, *Journal of structural Engineering* 139 (7) (2013) 1112–1123.
- [49] D.-T. R. Pasala, A. A. Sarlis, S. Nagarajaiah, A. M. Reinhorn, M. C. Constantinou, D. Taylor, *Seismic response control of structures using a novel adaptive passive negative stiffness device*, MCEER, 2013.
- [50] N. Attary, M. Symans, S. Nagarajaiah, A. M. Reinhorn, M. C. Constantinou, A. A. Sarlis, D. R. Pasala, D. Taylor, Performance evaluation of negative stiffness devices for seismic response control of bridge structures via experimental shake table tests, *Journal of Earthquake Engineering* 19 (2) (2015) 249–276.

- [51] Q. Liu, Z. Hou, Y. Zhang, X. Xu, D. Jiang, Some practical regards on the application of the physics-informed sparse identification for strongliness, *Communications in Nonlinear Science and Numerical Simulation* 143 (2025) 108610.
- [52] Q. Liu, Q. Li, D. Jiang, On efficiency and accuracy of sparse identification of bistable nonlinear energy sink chains, *International Journal of Dynamics and Control* 12 (12) (2024) 4413–4422.